PONTIFÍCIA UNIVERSIDADE CATÓLICA
DO RIO DE JANEIRO

Carlos Eduardo Orihuela Vargas

Millimeter Wave Measurements for a Range of Frequencies from 26.5 GHz to 40 GHz

Tese de Doutorado

Thesis presented to the Programa de Pós–graduação em Engenharia Elétrica of PUC-Rio in partial fulfillment of the requirements for the degree of Doutor em Ciências – Engenharia Elétrica.

Advisor: Prof. Luiz Alencar Reis da Silva Mello

Co-advisor: Prof. Glaucio Lopes Ramos

Rio de Janeiro

August 2019

Carlos Eduardo Orihuela Vargas

Millimeter Waves Propagation for a range of frequencies from 26.5 GHz and 40 GHz

Thesis presented to the Programa de Pós-Graduação em Engenharia Elétrica of PUC-Rio in partial fulfillment of the requirements for the degree of Doutor em Engenharia Elétrica. Approved by the Examination Committee.

Prof. Luiz Alencar Reis da Silva Mello
Advisor
Centro de Estudos em Telecomunicações – PUC-Rio

Prof. Glaucio Lopes Ramos
Co-Advisor
UFSJ

Prof.ª Leni Joaquim de Matos
UFF

Prof. Pedro Vladimir Gonzalez Castellanos
UFF

Prof. José Ricardo Bergmann
Centro de Estudos em Telecomunicações – PUC-Rio

Dr. Carlos Vinicio Rodríguez Ron
INMETRO

Dr. Rodolfo Saboia Lima de Souza
INMETRO

Rio de Janeiro, August 28th, 2019.

Carlos Eduardo Orihuela Vargas

Received the B.S degree in Telecommunications Engineering from Universidad Católica San Pablo, Bolivia, in 2011, and the M. S. degree in Electrical Engineering from Pontifíca Universidade Católica do Rio de Janeiro, Brazil, in 2015.

To my daughter Lara,

my wife Roxana,

my parents, Irma and Eduardo

my brother Roberto and his family.

Acknowledgment

I thank to God for accompanying and guiding me throughout my entire life, for having been my strength in times of weakness and for giving me a life full of learning, experiences and above all happiness.

To my professor, Luiz da Silva Mello, for all the support offered along these 4.5 years, for his confidence in me, for the valuable suggestions and criticisms he gave me during the preparation of this thesis. To my co-counselor and friend Glaucio Lopes, for all advices and support during this work.

To my wife Roxana, for being by my side during this long journey, supporting and encouraging me always and in every moment.

I thank my parents, Irma and Eduardo, for supporting me at all the time, for the values they gave me and for giving me the opportunity to have the best education as possible in the course of my life. Especially for being a great example of life to be followed.

To my brother, Roberto, for being part of my life, for being an example of professional development to follow, and for being my adviser in every new step of my life.

To my friends, Mauricio, Ariel, Lisseth, Alan, Diego, Junior, Jennifer, Andy, Marcelo, Teddy and all CETUC, for being an important part of my life, and for playing the role of a family during this period, thanks for the support, understanding and, above all, friendship.

To all the friends and family that in one way or another have encouraged or helped me during this time.

Abstract

The millimeter wave term refers to the portion of the electromagnetic spectrum with frequencies between 30 and 300 GHz corresponding to wavelengths from 10 to 1 mm, that commercially is known as millimeter waves frequencies.The characteristics of millimeter waves differ from microwaves and infrared, and these differences make millimeter wave systems ideal candidates for some applications. In the past years, the lack and high cost of sources, devices, components and adequate instrumentation for this frequency range have caused a low progress. However, in the currently planning of the new generation of mobile communication system this is changing, and devices in this frequency range are being marketed worldwide. The frequency range proposed for new generation of mobile communication varies from 24.25 GHz to 86 GHz. In Brazil, the bands proposed are 24.25 GHz to 27.5 GHz and also from 27 GHz to 40 GHz. In this work, we will explore the range from 26.5 GHz to 40 GHz, due to equipment limitations. This frequency range is already being studied by several researchers. However, there is not extensive literature on measurement results in different environments or with different materials. This work will present results of penetration loss measurements in different materials, and the reflection coefficients for each material. Also, outdoor measurements made in the university campus will be presented and an improved path loss prediction method developed. Indoor measurements results, made in the Center of Studies in Telecommunications and in another building in the campus will also be presented.

Keywords

Millimeter waves, outdoor measurements, indoor measurements, penetration loss, reflection.

Resumo

O termo de ondas milimétricas refere-se à porção do espectro eletromagnético com frequências entre 30 e 300 GHz, correspondente a comprimentos de onda de 10 até 1 mm. As características das ondas milimétricas diferem das microondas e das ondas infravermelhas, e são estas diferenças que fazem com que um sistema de ondas milimétricas seja o candidato ideal para algumas aplicações. Em anos passados a falta e o alto custo de fontes, dispositivos, componentes e instrumentação adequada para esta faixa de frequências, levaram a um progresso muito lento nesta área. Atualmente, com o planejamento da nova geração de comunicações móveis, isto está mudando e dispositivos nesta faixa de frequências estão sendo comercializados mundialmente. A faixa de operação pensada para a nova geração de comunicações móveis 5G vai de 24.25 GHz até 86 GHz. No Brasil, as faixas consideradas são de 24.25 GHz até 27.5 GHz e possivelmente de 37 GHz até 40 GHz. Neste trabalho vamos explorar a faixa de frequências entre 26.5 GHz e 40 GHz. Esta faixa já está sendo estudada por vários pesquisadores, porém ainda não existe muita literatura sobre resultados de medições em diferentes ambientes compostos por diferentes materiais. Neste trabalho serão apresentados resultados de medições de perda de penetração e coeficientes de reflexão em materiais de construção usuais. Também serão apresentados resultados de medições de perda de propagação em ambientes abertos (*outdoor)*, realizadas no campus da PUC-Rio, e um modelo de predição desenvolvido com base nos resultados. Resultados de medições em ambientes fechados (*indoor*), realizadas no Centro de Estudos em Telecomunicações e num prédio da mesma universidade, também serão apresentados ao final desta tese.

Palavras-chave
Ondas milimétricas, medidas outdoor, medidas indoor, perda de penetração, reflexão.

Table of contents

List of figures

List of tables

1
Introduction

It was difficult to foresee how wireless communications would become an essential part of our personal lives and work nowadays, when Martin Cooper, a Motorola researcher and executive, made the first mobile telephone call in 1973. Nowadays wireless communications are a medium to transport our work, education and entertainment wherever we want without any physical connection, making this technology pervasive, with over 5 billon cellphones globally.

However, since first mobile telephone call was made 45 years ago, computer clock speeds have increased from less than 1 MHz to 5 GHz, more than three orders of magnitude. Memory and storage sizes of computers have increased around seven orders of magnitude. During this time, mobile communication was limited by operating carrier frequency. Cellular mobile systems were allocated principally in the spectrum known as UHF band (Ultra High Frequencies), which corresponds to around 1 per cent of the whole regulated spectrum. For a long time, this range of frequencies between 300 MHz and 3 GHz was considered as the ideal range for the mobile networks. Wavelengths in this range are sufficiently short, allowing smaller antennas that can fit into small devices but big enough to contour and penetrate obstacles such as buildings and foliage. Even if transmitted with low power, the waves in this range of frequencies can travel reliably for up to few kilometers.

Nowadays, electromagnetic spectrum is congested due to the high increase in the use of mobile devices like smartphones, tablets, smart tv's, smart watches and many others. According to Cisco [1][1] there will be around 28 billion networked devices in 2022, up from 17.5 billion in 2017; mobile data traffic will reach 77.5 Exabytes per month in 2022, up from 11.5 Exabytes per month in 2017, and video streaming will be 79% of this traffic. On the other hand, according to Ericsson [3], during the Olympic games in Rio de Janeiro, streaming video (20%),

web browsing (20%) and social media (27%) dominated the data traffic. At the world championships for aquatic sports in Hungary in 2017 there was a similar distribution. However, the social networking and video streaming categories were even more dominant with 39% and 31%, respectively.

Currently, Tv broadcasting operates in the VHF (Very High Frequency) and UHF (Ultra High Frequency) bands, whereas cellphones, tablets, laptops and other wireless devices operate in frequencies between 700 MHz and 6 GHz. The millimeter wave spectrum, from 30 to 300 GHz, allocates some services like military communications, radar, and backhaul, but the utilization is not really high [4]. Many countries do not have regulations above 100 GHz. Millimeter waves were not used before because of many factors such as slow standardization process and slow spectrum regulations, the big amount of investment needed considering the existing and expanding infrastructure required to carry large bandwidths and, especially, the cost of designing, fabricating and deploying technologies working at these frequencies. Fortunately, this is all about to change.

With a large amount of spectrum available in the millimeter wave band, channel bandwidths of 1 GHz or more could be offered to the user in mobile communications [5]. The use of millimeter waves is just beginning and will continue growing due to the need of higher data rates to download/upload media with lower delays and with a constant connectivity on wireless devices. The 28 GHz, 38 GHz and 70-80 GHz are frequencies especially promising for next-generation cellular systems. Although the millimeter waves band is formally defined as the spectrum between 30 and 300 GHz, the industry considers the term millimeter waves to denote all frequencies between 10 and 100 GHz.

When part of the electromagnetic spectrum is globally allocated for a service, widespread adoption and commercial success is inevitable. This is already demonstrated with the IEEE 802.11b WLANs and its other versions IEEE 802.11a, IEEE 802.11g, IEEE 802.11n, IEEE 802.11ac [5]. This occurred because there was an international agreement for the use of 2.4 GHz and 5 GHz bands, and recently for 60 GHz for the last version of this technology IEEE 802.11ad, so that all products for this service can be sold and used globally, increasing new investments in new products for this technology, which means a wide range of options at

convenient prices for the end user. Then, it is clear that this kind of agreements must be made for the new generation of wireless mobile communication system, if we want to be successful in this promising technology that will allow massive data rates and new capabilities. Just like WLAN products have moved from the carrier frequencies of 2.4 GHz to 5 GHz and now to 60 GHz, mobile industry should be following this trend.

Some years ago, many regulatory offices of different countries rejected the use of millimeter wave frequencies due to the unfavorable propagation characteristics and the commercial cost of circuitry in this frequency range. These unfavorable propagation characteristics result in short coverage distances, principally caused by oxygen absorption, especially in the particular frequencies like 60 GHz where atmospheric loss is around 15 dB/km. Additionally millimeter wave links have high free space path loss, high penetration loss through obstacles and need directional communication due to high gain antenna requirements.

However, this panorama is changing in our days with the introduction of low-cost silicon circuit solutions. Furthermore, poor propagation characteristics of the millimeter waves are now surmountable or even seen as advantages. For example, the 15 dB/km atmospheric loss in 60 GHz represent a low atmospheric loss if a 100 to 200-meter cell radius is considered. Additionally, the shift from long-range communications to short-range communications would allow a strong reuse of frequencies. Even more, the high atmospheric losses seen at 60 GHz, practically disappears at other frequencies such as 28, 38 or 72 GHz, so these frequencies have similar propagation characteristics as the current ones. Recent research found that urban environments produce a lot of reflection and scattering when frequencies around 28 GHz or more are used for communication. Therefore, these multiple reflections can be highly exploited through spatial processing, intelligent antennas, beamforming and other technologies to increase the received signal power in non-line of sight (NLOS) environments. In this way, millimeter waves became a good option for the future generation of mobile communications [6].

The first short-range commercial application with millimeter waves was provided recently and the wireless personal area networks (WPAN) specifications are WirelessHD, IEEE 802.11ad (WiGig) and IEEE 802.15.3c, all of them using the 60 GHz band. The main application of WPAN is replace the use of the high definition interface (HDMI) to provide high bandwidth connections between devices wirelessly. Nowadays, every new device is more portable thanks to the integration of silicon circuitry and millimeter wave frequencies offer a large spectrum available for allowing media streaming and avoiding high data compressions, which are very common at lower frequencies where available spectrum is reduced. Low data compressions reduce signal processing and coding circuitry requirements allowing devices with less complexity, which lead to lower costs to the end users.

The Wireless Gigabit Alliance (WiGig) incorporated both WPAN and WLAN capabilities in the standard IEEE 802.11ad, and many devices like laptops, tablets and smartphones compatibles with this technology are already being offered globally. The Universal Serial Bus (USB) standard showed how compatibility of a technology in different devices play an important role, leading to the massive use. The 60 GHz technologies could be ready to play this role in high definition multimedia systems. Also, many companies are using millimeter waves frequencies to provide high speed line-of-sight (LOS) connections between base stations and backbone networks, reducing the need of high cost fiber optic connections.

Although millimeter waves are enabling new wireless and indoor services, many experts doubt that these frequencies can support cellular links. An important concern is that millimeter wave mobile networks will not be able to provide full coverage, particularly in outdoor environments in cities, because they cannot always guarantee a line-of-sight connection from a base station to a device. If, for example, a smartphone user suddenly passes behind a tree or other structure, a millimeter-wave transmission would probably not be able to penetrate those obstacles. However, as they reflect in solid materials, such as buildings, signs, and even people, the waves scatter throughout the whole environment, increasing the probability to catch one of these signals at the receiver even with NLOS communication.

Like any wireless system, the probability of a lost connection increases as the receiver moves away from the transmitter. Some studies show that the signal loss begins at around 200-300 meters. This limited range may have been a problem for previous generations of cellular systems, where a typical cell radius extends up to kilometers. In the last decade however, carriers have decreased this cell size significantly in order to expand capacity. Especially in dense urban centers, the use of small cells and compact base stations is starting to be used, with ranges not exceeding 100-200 meters.

Millimeter wave spectrum would allow higher channel bandwidths than the actual 20 MHz offered by 4G LTE, providing a large increase in capacity and reducing latency. This untapped spectrum can be used in mobile communications systems to increase the actual radio spectrum bands which are already saturated. Combining the cost-effective CMOS technology that can now operate in these range of frequencies and the use of high gain antennas reinforces the viability of millimeter wave communications [7]. Deploying mobile communications in licensed spectrum such as 28 GHz, 38 GHz or even 72 GHz guarantees the quality of service. Thus, it is important to acquire knowledge of how millimeter waves at these frequencies propagate in indoor and outdoor environments; how reflective are these waves are at different types of materials that exist in our daily environment; what is the level of penetration loss through these materials in this frequency range; and how rain will affect or not short-range millimeter wave links.

In this work, millimeter waves propagation was studied for a range of frequencies from 26.5 GHz to 40 GHz. Penetration loss through construction materials and the reflection coefficient for the same materials were obtained. Indoor and outdoor links were deployed inside the campus of PUC-RIO, and the propagation loss obtained from measurements.

In Chapter 2, a brief history of the evolution of mobile technologies is described to introduce the new generation 5G, where millimeter waves are the focus of recent research. Chapter 3 includes penetration loss and reflection measurements and results. In Chapter 4 describes path loss models. Chapter 5 presents outdoor measurements in a university campus, where antenna heights and vegetation depth

are considered for analysis. Chapter 6 includes indoor measurements in the Centre for Telecommunications Studies and also in a corridor at Leme Building. Chapter 7 summarize the conclusions of this work.

2

Mobile Communication Systems Evolution

2.1   Introduction

The possibility of communicating with other people through radio waves while they are moving was demonstrated by Guglielmo Marconi in 1897, when he obtained constant communication with ships on the English Channel. Since then new methods of wireless communication have been investigated around the world.

The first public mobile telephone service was introduced in 1946 in the biggest American cities. It was composed by a large tower to cover distances around 50 km, it was a FM push-to-talk telephone system with half duplex mode, it means that just one user could talk in a determinate time. The RF bandwidth of this system was 120 kHz, but just 3 kHz of spectrum was used for communication. This large RF bandwidth was because on that time it was hard to produce tight RF filters and low noise amplifiers. In 1950, the Federal Communication Commission (FCC), doubled the number of channels and thanks to the improvement of technology the RF bandwidth could reduce to 60 kHz and by mid 1960's, to 30 kHz. With the introduction of the Improved Mobile Telephone Service (IMTS) between 1950's and 1960's, telephone companies started to offer full duplex, auto-dial and auto-trunking phone systems [8].

Initially, mobile systems aimed to reach large coverage areas through a single high-power transmitter and used the access technique known as Frequency Division Multiple Access (FDMA), in which each user is allocated at a different frequency. Although this approach provided very good coverage, the number of users was limited. As an example of the low capacity, by 1976 the Bell Mobile Phone service for New York City had only twelve channels and could attend only 543 paying customers. They had a waiting list of over 3700 people [8] even being

a poor service with many call blockings. With the high demand for mobile services, the need for a restructuring of the radio telephone system was obvious in order to achieve higher capacity and maintain the large coverage areas in the same available limited spectrum. With this, the first generation of cellular communication systems emerged.

2.2 The Evolution of Cellular Systems

2.2.1 First Generation of Cellular Systems

In 1968 AT&T Bell Laboratories proposed the cellular concept to the FCC [9], but technology to implement this system was not available until late 1970's.

In 1979, the world's first cellular system was implemented in Japan by Nippon Telephone and Telegraph company (NTT), with 600 FM duplex channels (25 kHz for each one-way link) in the 800 MHz band.

In 1983, the FCC finally allocated 666 duplex channels (40 MHz of spectrum in the 800 MHz band, each channel had a bandwidth of 30 kHz) for the US Advanced Mobile Phone System (AMPS) [10]. As demand for cellular telephone service increased rapidly, in 1989, the FCC allocated 10 MHz more for cellular communications. This system used large cells and omnidirectional base station antennas and it was deployed in Chicago to cover approximately 3380 square kilometers. After many tests, it was found that the AMPS 30 kHz channel required a signal-to-interference ratio (SIR) of 18 dB to have a good performance. The smallest reuse factor (N) which satisfies this requirement using 120 degree directional antennas is N = 7, this seven-cell reuse pattern was adopted. To increase capacity in AMPS systems, Motorola developed Narrowband AMPS (N-AMPS), in 1991, and 10 kHz channels could provide three users in a 30 kHz AMPS channel.

In Europe, the Nordic Mobile Telephone system (NMT 450) was developed in 1981 for the 450 MHz band and used 25 kHz channels. After that, in 1985, the European Total Access Cellular System (ETACS) was deployed and it was very similar to the US standard AMPS. The only difference was the channel bandwidth,

a little smaller (25 kHz instead of 30 kHz) which resulted in a small degradation of the signal noise ratio (SNR) and the coverage range. In Germany, a cellular standard called C-450 was introduced in the same year. The first-generation European cellular systems were incompatible with each other because of the different frequencies and communications protocols used.

Table 2.1 presents a comparison between first analog cellular radio systems throughout the world.

FIRST GENERATION				
SYSTEM PARAMETERS	AMPS (USA)	TACS (UK)	C450 (ALEMANHA)	NTT (JAPÃO)
Operation Frequency (MHz) - Base Station - Mobile	870 - 890 825 - 845	935 - 960 890 - 915	461 - 165 451 - 455	870 - 885 825 - 840
Space between TX and RX bands (MHz)	45	45	10	5
Channel Bandwidth (kHz)	30	25	20	25
Channels	666 (NES) 832 (ES)	1000	222	600
Coverage (km)	2 - 25	2 - 20	5 - 30	5 - 10
Transmission rate (kbps)	10	8	5,28	0,3

Table 2.1: First Generation of cellular systems

2.2.2 Second Generation of Cellular Systems

As the growth in demand for cellular service was very high, an increase in capacity was essential. Then, after a lot of research and comparison by major cellular manufacturers, in the late 1980's, the United States Digital Cellular System (USDC) was developed to support more users than AMPS. USDC is a time division multiple access (TDMA) system which offers as much as six times the capacity of AMPS [11]. As AMPS, USDC uses the same 45 MHz of separation between

forward and reverse channels. The combination of AMPS-USDC was standardized as Interim Standard 54 (IS-54) by the Electronic Industries Association and Telecommunication Industry Association (EIA/TIA) in 1990 [12], later upgraded to IS-136, IS-54 uses analog control channels and IS-136 uses digital control channels. The USDC was designed to be compatible with AMPS, in that way base stations and mobile units could be work in both AMPS and USDC. USDC is also known as North American Digital Cellular (NADC), as it was installed in Mexico and Canada.

Because of incompatibility of the first generation of cellular systems in Europe, a second generation of cellular system was developed, under the name of Global System for Mobile (GSM) in the mid 1980's and introduced into the European market in 1991 [13]. By the end of 1993, several countries of South America, Asia, and Australia had adopted GSM.

From the user's point of view, the most remarkable feature is the introduction of GSM Subscriber Identity Module (SIM), which is a memory device that stores information like the subscriber's identification number, networks available for use, privacy keys and other user information. SIM cards are removable and portable and can be used in any GSM phone. A second remarkable feature is privacy. Unlike analog systems, in which the signal could be monitored easily, in GSM it is virtually impossible to eavesdrop on a GSM radio transmission, since transmission in GSM is encrypted and key is only known by cellular carrier and change periodically.

GSM uses two 25 MHz bands with a spectrum separation of 45 MHz, FDD and a combination of TDMA and FHMA (Frequency Hopped Multiple Access) schemes to provide access to multiple users. The channel bandwidth is 200 kHz and every channel is shared in time by 8 users.

In 1993, a US digital cellular system based in Code Division Multiple Access (CDMA) was standardized as Interim Standard 95 (IS-95) by the US Telecommunications Industry Association (TIA) [14]. As IS-136, IS.95 was designed to be compatible with analog cellular system (AMPS). IS-95 allows each

user within the cell to use the same radio channel, and users in adjacent cells can operate in the same radio channel, since this is a direct sequence spread spectrum CDMA system. Frequency planning is not more needed with the use of CDMA. Each IS-95 channel occupies 1.25 MHz of the spectrum on each one-way link and forward and reverse channels are separated by 45 MHz.

In Japan, the Pacific Digital Cellular (PDC) standard was developed in 1991 [15]. It is very similar to the IS-136 American standard. FDMA and TDMA are used to provide three time slots for three users in a 25 kHz channel. Forward and reverse channels were separated by 130 MHz in the low PDC band and by 48 MHz in the high PDC band.

Even with relatively small user data rates, 2G standards are able to support limited Internet browsing and sophisticated short message capabilities using a circuit switched approach. Short messaging service (SMS) is a popular feature of GSM which allows users to send messages in real time to another user. A comparison between the principal standards of this generation is presented in Table 2.2

SECOND GENERATION			
SYSTEM PARAMETERS	IS-54 IS-136 (USA)	GSM (EUROPA)	IS-95 (USA)
Access technique	TDMA	TDMA	CDMA
Operation Frequency (MHz) - Base Station - Mobile	869 - 894 824 – 849	935 - 960 890 – 915 1710 - 1785 1805 - 1880	869 – 894 869 - 894
Duplexing	FDD	FDD	FDD
Channel Bandwidth (kHz)	30	200	1250
Modulation	DQPSK	GMSK	BPSK/QPSK
Voice Channels per carrier	3	8	-
Transmission Rate (kbps)	48,6	207,833	-
Frame length (ms)	40	4,615	20

Table 2.2: Second Generation of cellular systems

In order to achieve higher Internet data rates, 2G standards were upgraded and this new generation of cellular systems was called 2.5G. There were principally two paths for this evolution. One was based in 2G TDMA standards, whith 3 solutions presented: (a) High Speed Circuit Switched Data (HSCSD); (b) General Packet Radio Service (GPRS); and (c) Enhanced Data Rates for GSM Evolution (EDGE). A second path was designed for 2G CDMA (IS-95) and was called (IS-95B).

HSCSD is a circuit switched technique that allows a single user to use consecutive time slots instead of just one as GSM TDMA, in order to obtain higher speed data rates. HSCDS moderated the error control coding algorithms of GSM increasing the data rate to 14.4 kbps as compared with the original 9.6 kbps in GSM. When using four consecutive time slots, HSCDS can provide a rate up to 57.6 kbps to the user. This standard is ideal for dedicated streaming Internet access or real-time web sessions. Carrier just needs to implement software change at existing GSM base stations.

GPRS is a packet-based data network ideal for non-real Internet usage, emails, faxes, and asymmetric web browsing, in which downloads are much greater than uploads. It supports multi-user network sharing individual channels and time slots, allowing much more users than HSCSD. When all eight time slots of a GSM channel are dedicated to GPRS, a user can achieve as much as 171.2 kbps (eight time slots multiplied by 21.4 kbps from the original GSM data rate). GPRS was originally designed to provide a packet data access over GSM networks, but IS-136 operators requested to extend GPRS to IS-136 too. As any packet network, the data throughput decreases with more users and also when propagation conditions are poor.

EDGE was developed for GSM and IS-136 operators to have a common technology path for eventual 3G high speed data access, but was initially proposed by GSM community. GSM standard requires addition of new hardware and software in its base stations to upgrade to the EDGE standard. EDGE introduces a new digital modulation format, 8-PSK (octal phase shift keying) which is used in addition to the GMSK modulation of GSM. EDGE allows nine different air

interface formats, known as multiple modulation and coding schemes (MCS). Each MCS could decide if GMSK (low data rate) or 8-PSK (high data rate) is used according to the demands in the network. Because of higher data rates and many formats for error control, the coverage of EDGE is smaller than HSDRC or GPRS. When EDGE uses 8-PSK modulation without any error protection and all eight time slots of GSM channel, a data rate of 547.2 kbps can be provided. In practice, combining practical network connection issues and error control coding requirements, a data rate up to 384 kbps is obtained.

The IS-95 standard was upgraded to IS-95B. This upgrade provides high speed packet and circuit switched data access on a common CDMA channel by dedicating multiple orthogonal user channels for specific users and specific purposes. Originally, IS-95 had data rates of 9.6 kbps but never was commercialized. In practice, this was improved with the standard IS-95A with data rates of 14.4 kbps. IS-95B allows the user to use eight different orthogonal channels at the same time and achieve a throughput of 115.2 kbps (14.4 kbps x 8). However, in practice, a data rate about 64 kbps is achieved. IS-95B offers a harder and more efficient handoff procedure.

2.2.3 Third Generation of Cellular Systems

The Universal Mobile Telecommunications System (UMTS) was presented by the European Telecommunications Standards Institute (ETSI) to ITU in 1998 for consideration as a world standard. It was designed to provide a high capacity upgrade path for GSM. This standard uses wideband CDMA (W-CDMA). The 3G W-CDMA air interface standard was designed for "always-on" packet based in wireless service, in that way, computers, entertainment devices and telephones can share the same wireless network and be connected to the Internet, wherever they are and whenever they want. It supports packet data rates up to 2.048 Mbps per user (if stationary), allowing high quality of service, multimedia, streaming audio and video.

W-CDMA requires a minimum of 5 MHz of spectrum and it is compatible with GSM, IS-136, PDC, GPRS and EDGE. W-CDMA 5 MHz channels support

between 100 and 350 voice calls at the same time, depending on the propagation conditions, user velocity, antenna polarizations and antenna sectoring. The High-Speed Packet Access (HSPA) standard is the result of the use of two mobile telephone protocols, the High-Speed Downlink Packet Access (HSDPA) and the High-Speed Uplink Packet Access (HSUPA). It extends and improves the performance of existing W-CDMA protocols, with data rates that can reach up to 14 Mbps in the downlink and 5.8 Mbps in the uplink.

CDMA-2000 was developed to increase data rates of IS-95, IS-95A and IS-95B, therefore it is compatible with them allowing operators to introduce 3G capabilities without having to change base stations or spectrum. The first 3G CDMA air interface, CDMA-2000 1xRTT uses a single 1.25 MHz channel (RTT means Radio Transmission Technology). It supports data rate up to 307 kbps for a user in packet mode and typical throughput rates up to 144 kbps per user. CDMA-2000 1xEV is an evolutionary advancement for CDMA, originally developed by Qualcomm Inc., which is proprietary of high data rate (HDR) standard and implemented this standard to IS-95, IS-95B and CDMA-2000.

CDMA-2000 1xEV can install channels with data only (CDMA-2000 1xEV-DO) or with data and voice (CDMA-2000 1xEV-DV). CDMA-2000 1xEV-DO dedicates the radio channel only to data users and provides speeds greater than 2.4 Mbps on a particular CDMA channel. CDMA-2000 1xEV-DV can offer data rates up to 144 kbps. After that, the CDMA-2000 3xRTT standard was presented and uses three adjacent 1.25 MHz radio channels together, providing 2Mbps data rates per user.

The China Academy of Telecommunications Technology (CATT) and Siemens Corporation submitted a 3G standard proposal in 1998, based on Time Division Synchronous Code Division Multiple Access (TD-SCDMA) and was accepted in 1999. TD-SCDMA combines TDMA and TDD techniques to provide data-only in GSM network. A packet data up to 384 kbps is provided to users in 1.6 MHz channels.

2.2.4 Fourth Generation of Cellular Systems

LTE (Long Term Evolution) or the E-UTRAN (Evolved Universal Terrestrial Access Network), introduced in 3GPP R8 [16], is the access part of the Evolved Packet System (EPS). The main requirements for the new access network are high spectral efficiency, high peak data rates, short round trip time as well as flexibility in frequency and bandwidth.

The Evolved Packet System (EPS) is purely IP based. Both real time services and datacom services will be carried by the IP protocol. LTE is based on OFDMA (Orthogonal Frequency Division Multiple Access) and in combination with higher order modulation (up to 64QAM), large bandwidths (up to 20 MHz) and spatial multiplexing in the downlink (up to 4x4), can achieve high data rates. The highest theoretical peak data rate on the transport channel is 75 Mbps for uplink, and for downlink, using spatial multiplexing, the rate can be as high as 300 Mbps.

The LTE access network is very simple. It only has base stations and evolved NodeB (eNB) generating a flat architecture. There is no centralized controller, and the eNBs are normally inter-connected via the X2-interface and all of them to the core network by the S1-interface. In this way, intelligence of the system is distributed in all base stations making a faster system since a time for a handover is not more necessary. For an end-user, the connection in real time is crucial in many cases, especially in on-line gaming, video conferences and other services.

LTE is developed for a number of frequency bands ranging from 700 MHz up to 2.7 GHz. The available bandwidths are also flexible starting with 1.4 MHz up to 20 MHz. LTE is developed to support both the time division duplex technology (TDD) as well as frequency division duplex (FDD). In R8 there are 15 bands specified for FDD and eight bands for TTD. In R9 [17] four bands were added for FDD. Also added in R9 were, for example, Multimedia Broadcast Multicast Service (MBMS), and Home eNB (HeNB).

MBMS is used to provide broadcast information to all users, for example advertisement, and multicast to a closed group subscribing to a specific service.

HeNBs are introduced mainly to provide coverage indoors, in homes or offices. The HeNB is a low power eNB that will be used in small cells named femtocells.

LTE Release10 [18] would provide higher bit rates in a cost-efficient way and, at the same time, completely fulfil the requirements set by ITU for IMT Advanced, also referred to as 4G. The main new functionalities introduced in LTE-Advanced are Carrier Aggregation (CA), enhanced use of multi-antenna techniques and support for Relay Nodes (RN). With these new features LTE-Advanced increased peak data rates to 3 Gbps for download and 1.5 Gbps for upload. The spectral efficiency is 30 bps/Hz comparing the 15 bps/Hz in Release 8.

2.2.5 Fifth Generation of Cellular Systems

Mobile communication, along with the internet, has been a revolutionary technology in the history. This technology has lived longer than any previous technology. It can be said that at least 50% of the world's people are using this technology according to Dr. Farooq Khan, president of the Samsung Research Center in America.

This technology has been adapted to offer more services to users. A few years ago, even now in some developing countries, in order to be able to make bank transfers, the user usually takes a long time in these bank branch operations, but with the ease of today's mobile communications, this can only be done in a few minutes through our computer or our cell phone. In the same way, we can have information from our medical history without having to go to the hospital, or study at different universities without being present.

This type of services has increased the consumption of mobile services and is still increasing rapidly, leading data traffic to grow exponentially. According to 2017 Ericsson Mobility Report "by 2017 the mobile data traffic through smartphones grew 65% between Q3 2016 and Q3 2017, by November 2017 mobile data traffic was 11.5 Exabytes/month where 55% of this traffic was video; and we will achieve almost 103 Exabytes/month by 2023 where 75% will be video". A complete forecast of the mobile data traffic can be shown in Figure 2.5 [3]. According to 2017 Cisco VNI Forecast, by 2016 we had 17.1 billion networked

devices worldwide (2.3 devices per capita) and by 2021 there will be approximately 27.1 billon network devices in the world (3.5 devices per capita) [1][2]. Globally, the average mobile connection speed was 6,837 kbps in 2016 and will grow 3-fold from 2016 to 2021, reaching 20 Mbps in 2021.

Data Traffic – Smartphone
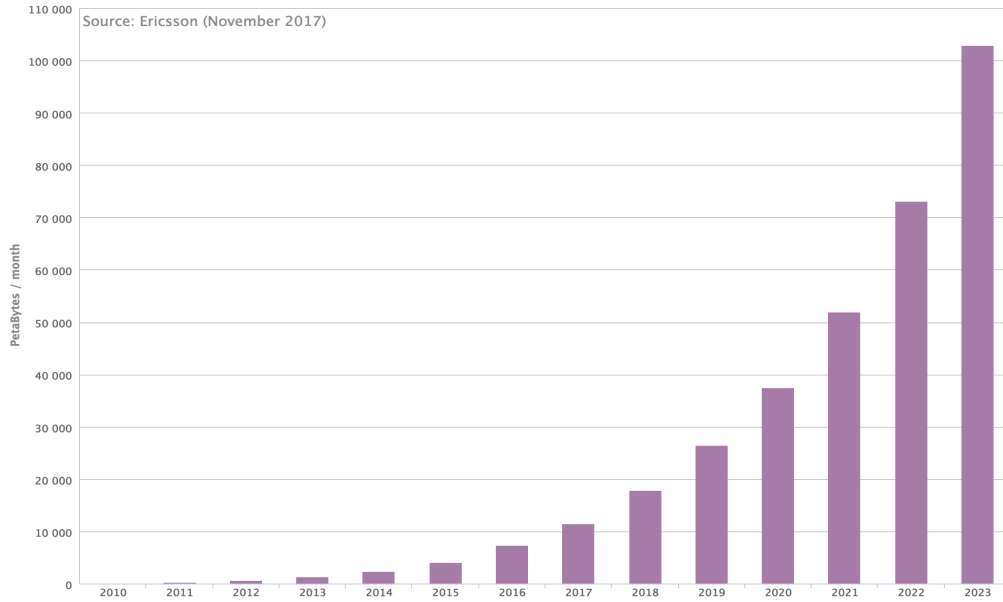
Figure 2.1: Mobile data traffic evolution in the world

The current fourth generation will not be able to support this type of demand in the next few years, as technological trends will lead to greater demand than the actual capacity of cellular networks. The behavior of mobile devices has changed drastically, and no one had any idea of this exponential growth before, so now we cannot think of a technology that only allows an increase of twice the current capacity, not even 10 times.

The new technology must be able to support 100 or 1000 times the current capacity to be able to cover capacity for the next 10, 15 years. In fact, this is not impossible. Other technologies, such as storage or computational processing, have experienced this kind of growth, up to millions of times in the last 30 years, so cellular networks can also have this kind of growth. It will not be easy, but it will have to be done. According to the Shannon's Law:

$$C = W \cdot log_2(1 + SNR) \tag{2.1}$$

where C is the channel capacity, W is the channel bandwidth and SNR is the Signal-Noise Ratio, the bandwidth is clearly a big factor to increase capacity in a cellular system, but until now every new generation, in general, involved three steps: improving spectral efficiency, increasing user bandwidth (limited by spectrum allocations) to provide higher traffic rates and enabling new services. The problem is that all radio communications, such as TV service, Radio, cellular communications, use the spectrum up to 3 GHz, which is a very limited spectrum and is already completely congested. Then, a solution to increase capacity in the next generations of cellular systems to cover the exponential demand of mobile communications is the use of higher frequencies and the millimeter wave band, where the antennas are smaller and especially, where the spectrum is much larger than the current one. Figure 2.6 shows the growth of subscriptions for every technology from 2010 to 2017 and a forecast to 2023 [3].
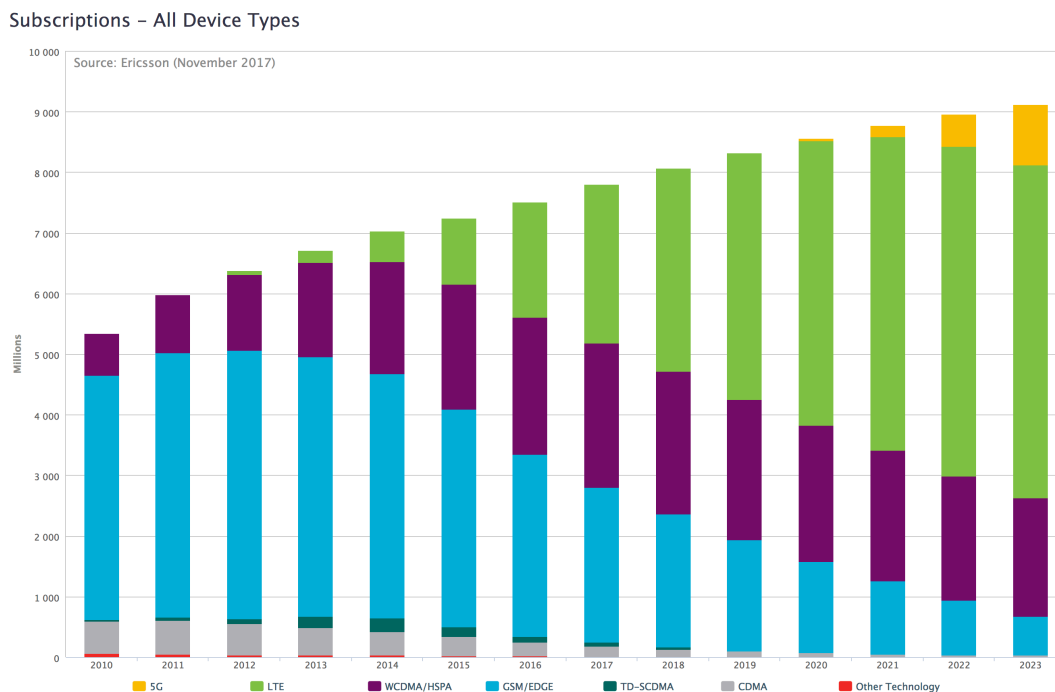
Figure 2.2: Worldwide subscriptions

2.3   Advantages and Disadvantages of Millimeter Waves

Millimeter waves offer, principally, more spectrum and high availability and goes from 30 GHz to 300 GHz, however, the industry named frequencies above 10 GHz as millimeter wave frequencies. Today, the UHF band (from 300 MHz to

3 GHz) is saturated. Government agencies around the world have allocated many services in this band and today there is few free spaces. The millimeter wave band partially solves the problem, providing more band for expansion allowing high data rates. Wireless communications in microwave frequencies and other low frequencies have limitations at about 1 Gbps. In the millimeter wave range, data rates could reach 10 Gbps or more.

The bad news is that while this spectrum gives us some margin for expansion, it is not useful for all types of wireless applications. It has its limitations and overcoming them has been a challenge. One of the main limitations of millimeter waves is the limited coverage range. Physics laws say that the shorter the wavelength, the shorter the transmission interval for a given power. The free space loss (L) in dB, is calculated by:

$$L = 92,4 + 20 \log f(GHz) + 20 \log D(km) \tag{2.2}$$

where f is the operating frequency and D is the distance between the transmitter and receiver. As an example, at a frequency of 30 GHz and a distance of 2 km, the loss of free space would be 128 dB. In addition, the atmosphere absorbs the millimeter waves, restricting the area of coverage. Rain, fog, and any air humidity make the signal attenuation very high, reducing transmission distances. Specific gas attenuation [19] and rain attenuation [20] are illustrated in Figures 2.7-2.8.
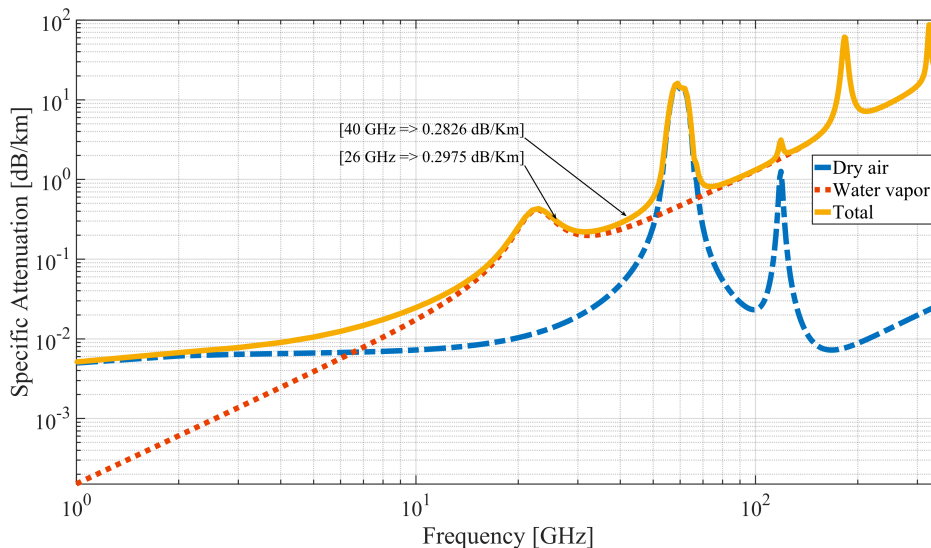
Figure 2.3: Specific gas Attenuation
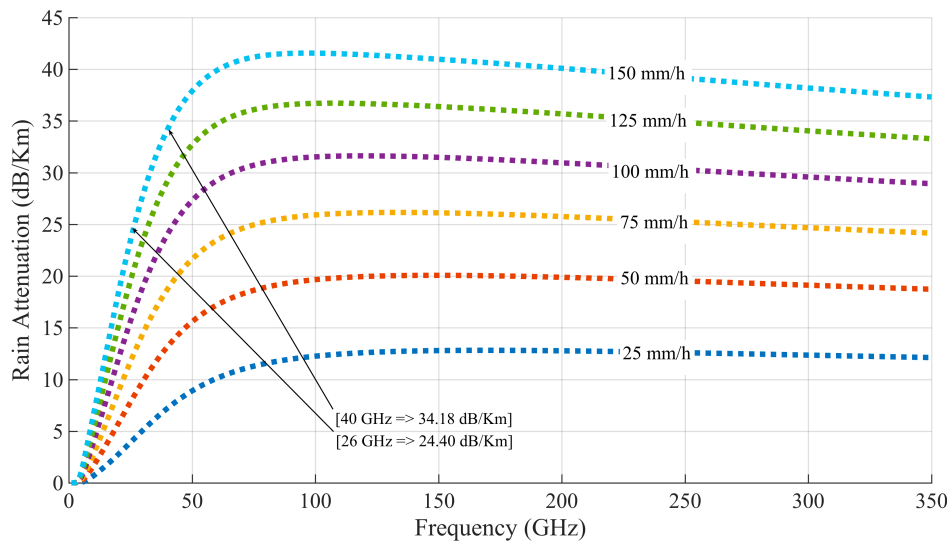
Figure 2.4: Rain Attenuation

Since the number of mobile users is increasing rapidly, cells of cellular systems trend to be smaller with every new generation in order to offer more capacity in certain areas, short coverage range of millimeter waves can be a benefit because it reduces interference with other nearby radio bases, the use of high gain antennas needed for a millimeter wave system, which are highly directional, also reduce interference. These narrow-beam antennas increase range power and also provide security since they prevent signals from being intercepted. Small size is another great advantage of millimeter wave equipment. As an example, a typical half-wave dipole with a frequency of 900 MHz is 16.6 cm long, but at 60 GHz is only about 2.5 mm. This means that the entire structure of the radio, including the antenna, may be very small which reduces manufacturing, installation and other costs. Then, if cell dimension reduces to a radius of 200 meters, then the 128 dB free space loss at 30 GHz reduces to 108 dB, which is comparable with actual systems operating around 3 GHz and with cell radius around 2 km. Specific attenuation and rain attenuation are also not really high considering this limit in cell radius.

2.4   Applications of Millimeter wave communications

The current commercial applications of wireless communications in the millimeter wave band are:

- Short range point-to-point links (< 2 km) for interconnection of local networks. The large unlicensed frequency band, available in the 60 GHz band, allows connection between local networks with up to 1.25 Gbps of data transfer rate, at relatively low costs;

- WLAN and WPAN to connect devices such as televisions, home theaters, video games, etc.; for the transmission of audio and video in high definition. This application allows the transmission of data at high rates, without the need of compression, reducing latency and complexity of the systems;

But, this is just the beginning, millimeter wave communications will also have a big impact on other technologies. Data centers may cut costs by employing millimeter wave communication links to interconnect the computers with high bandwidth, flexibility, and low power. Computational platforms may replace lossy, wired interconnects with high-speed wireless interconnects. Cellular systems may incorporate millimeter waves to provide higher bandwidths to solve the spectrum crunch by providing mobile networks, peer-to-peer data transfers, and backhaul in the same bands. Backhaul wireless links, broadband cellular communication, intra-vehicular communication, inter-vehicular communication, and aerospace communication are being the subject of actual research in all the world

3

Penetration Loss and Reflection at Millimeter Waves

3.1 Reflection and Transmission coefficients

If an incident wave with angle i is crossing through two different dielectric media, at the boundary between these two media, the energy is partially reflected with angle r to media one and partially transmitted to media two with angle t as shown in Figure 3.1. The nature of reflection varies with the direction of polarization of the electric field E-field.

Knowing that plane of incidence is the plane that contains the incident, reflected and transmitted rays. When E-field is perpendicular to the plane, polarization is perpendicular and when E-field is parallel to the plane, polarization is parallel [21].
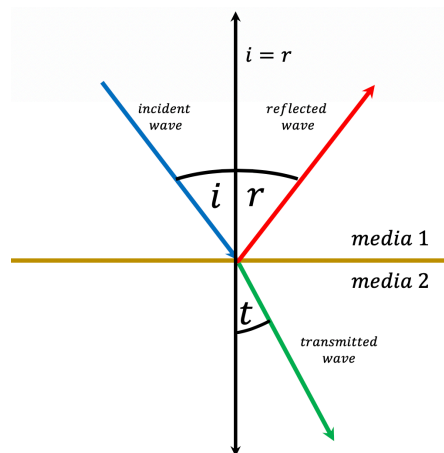
Figure 3.1: Geometry for calculating the reflection and transmission coefficients between two dielectrics

3.1.1 Perpendicular Polarization

When the electric field of a wave incident is perpendicular to the incident plane, the polarization is called perpendicular, as showed in figure 3.2

Figure 3.2: Perpendicular Polarization

where E is the electric field, H is the magnetic field i is the incident angle, r is the reflection angle and t is the transmission angle. From boundary conditions, equations 3.1and 3.2:

$$E_i + E_r = E_t \tag{3.1}$$

$$H_i \cos(i) - H_r \cos(r) = H_t \cos(t) \tag{3.2}$$

since $H = \frac{E}{\eta}$, where η is the intrinsic impedance, equation 3.2 results in:

$$\frac{E_i}{\eta_1} \cos(i) - \frac{E_r}{\eta_1} \cos(r) = \frac{E_t}{\eta_2} \cos(t) \tag{3.3}$$

$$\eta_2 E_i \cos(i) - \eta_2 E_r \cos(r) = \eta_1 E_t \cos(t) \tag{3.4}$$

If $i = r = \theta_1$; $t = \theta_2$; $E_t = E_i + E_r$

$$\eta_2 E_i \cos(\theta_1) - \eta_2 E_r \cos(\theta_1) = \eta_1 (E_i + E_r) \cos(\theta_2) \tag{3.5}$$

$$\eta_2 E_i \, cos(\theta_1) - \eta_1 E_i \, cos(\theta_2) = \eta_1 E_r \, cos(\theta_2) + \eta_2 E_r \, cos(\theta_1) \quad (3.6)$$

$$\frac{E_r}{E_i} = \frac{\eta_2 \, cos \, \theta_1 - \eta_1 \, cos \, \theta_2}{\eta_2 \, cos \, \theta_1 + \eta_1 \, cos \, \theta_2} = \Gamma_\perp \qquad (3.7)$$

Now, if we consider $i = r = \theta_1$; $t = \theta_2$; $E_r = E_t - E_i$ in equation 3.4 it is obtained:

$$\eta_2 E_i \, cos(\theta_1) - \eta_2 (E_t - E_i) \, cos(\theta_1) = \eta_1 E_t \, cos(\theta_2) \qquad (3.8)$$

$$\eta_2 E_i \, cos(\theta_1) + \eta_2 E_i \, cos(\theta_1) = \eta_1 E_t \, cos(\theta_2) + \eta_2 E_t \, cos(\theta_1) \qquad (3.9)$$

$$\frac{E_t}{E_i} = \frac{2\eta_2 \, cos \, \theta_1}{\eta_2 \, cos \, \theta_1 + \eta_1 \, cos \, \theta_2} = T_\perp \qquad (3.10)$$

$\Gamma_\perp$ is the reflection coefficient and $T_\perp$ is the transmission coefficient for perpendicular polarization.

3.1.2 Parallel Polarization

When the electric field of a wave incident is parallel to the incident plane, the polarization is called parallel, as showed in figure 3.3

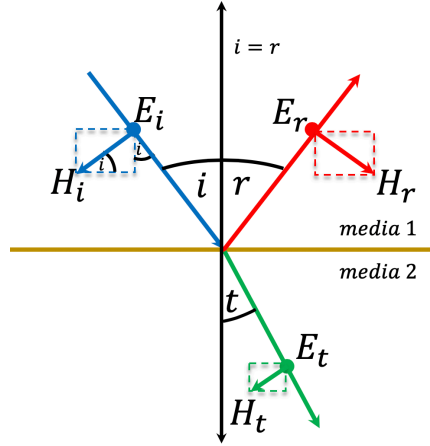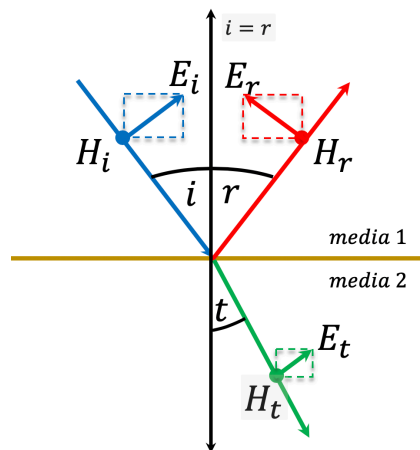**Figure 3.3:** Parallel Polarization

where E is the electric field, H is the magnetic field i is the incident angle, r is the reflection angle and t is the transmission angle. From boundary conditions, equations 3.11 and 3.12:

$$H_i + H_r = H_t \qquad\qquad (3.11)$$

$$E_i \cos(i) + E_r \cos(r) = E_t \cos(t) \qquad\qquad (3.12)$$

since $H_{i,t} = \frac{E}{\eta}$, and $H_r = -\frac{E}{\eta}$ where η is the intrinsic impedance, equation 3.11 results in:

$$E_t = \left(\frac{\eta_2}{\eta_1}\right)(E_i - E_r) \qquad\qquad (3.13)$$

if $i = r = \theta_1$; $t = \theta_2$; $E_t = \left(\frac{\eta_2}{\eta_1}\right)(E_i - E_r)$ and replace in 3.12, it is obtained:

$$E_i \cos(i) + E_r \cos(r) = \left(\frac{\eta_2}{\eta_1}\right)(E_i - E_r)\cos(t) \qquad\qquad (3.14)$$

$$\eta_1 E_i \cos(\theta_1) + \eta_1 E_r \cos(\theta_1) = \eta_2 E_i \cos(\theta_2) - \eta_2 E_r \cos(\theta_2) \qquad (3.15)$$

$$\eta_1 E_i \cos(\theta_1) - \eta_2 E_i \cos(\theta_2) = -\eta_1 E_r \cos(\theta_1) - \eta_2 E_r \cos(\theta_2) \qquad (3.16)$$

$$\frac{E_r}{E_i} = \frac{\eta_2 \cos\theta_2 - \eta_1 \cos\theta_1}{\eta_2 \cos\theta_2 + \eta_1 \cos\theta_1} = \Gamma_\parallel \qquad\qquad (3.17)$$

Now, if we consider $i = r = \theta_1$; $t = \theta_2$; $E_r = E_i - \left(\frac{\eta_1}{\eta_2}\right)E_t$ in equation 3.12 it is obtained:

$$E_i \cos(i) - \left(\frac{\eta_1}{\eta_2}\right)E_t \cos(r) + E_i \cos(r) = E_t \cos(t) \qquad\qquad (3.18)$$

$$\eta_2 E_i \cos(\theta_1) - \eta_1 E_t \cos(\theta_1) + \eta_2 E_i \cos(\theta_1) = \eta_2 E_t \cos(\theta_2) \qquad (3.19)$$

$$\frac{E_t}{E_i} = \frac{2\eta_2 \cos\theta_1}{\eta_2 \cos\theta_2 + \eta_1 \cos\theta_1} = T_{\parallel} \qquad (3.20)$$

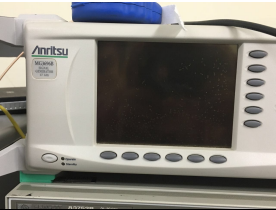$\Gamma_{\parallel}$ is the reflection coefficient and $T_{\parallel}$ is the transmission coefficient for parallel polarization.

3.2   Measurements setup

Several recent investigations, at millimeter wave, show that the human body, buildings and trees can be quite reflective at millimeter waves, compared to the microwave (1-6 GHz) band. This produces a high number of multipaths in the environment, with the waves bouncing off different materials along their path.

Reflected and scattered signals are part of the nature of millimeter waves and together with high gain antennas help to overcome the high free space path loss at these frequencies. However, despite the existence of a large number of multipaths along a link, obstructions such as trees, or even their leaves, metals, concrete walls and even glass with dark filters can considerably attenuate the millimeter wave signal [22][23][24][25]. One of the goals for the future generation of cellular systems will be to be able to process direct, reflected and scattered multipath components in order to have stable links over a region and in different environments. In this chapter, penetration loss measurements through different materials are presented as well as reflection measurements to obtain reflection coefficients. Our measurements setup equipment is listed in Table 3.1

Items	Description
Signal Generator	Anritsu MG3696B Frequency coverage from 2 to 65 GHz Output type V(f) Max Level Output: +3 dBm (20 to 65 GHz) A CW with a 0 dBm power level was used for all measurements.
1-meter cable for TX	Pasternak PE361 Insertion Loss (Max.): 2.40 dB (20 GHz) 3.61 dB (40 GHz)
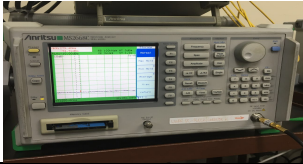
TX and RX Antennas	20 dBi gain with a horizontal half power beam width (HPBW) of 16.7 degrees and a vertical half power beam width of 18.3 degrees. Frequency operation: 26.5 to 40 GHz
1-meter cable for RX	Pasternak PE360 Insertion Loss (Max.): 2.47 dB (26 GHz) 3.19 dB (40 GHz)
Spectrum Analyzer	Anritsu MS2668C Frequency coverage from 9 kHz to 40 GHz Output type K(m) Average Noise Level: -101 dBm (26 to 40 GHz)
Antenna Tripods	Velbon Videomate 638 - Max elevation: 171 cm

Table 3.1: Measurements Setup

3.3 Penetration Loss Measurements

The first measurements were performed in a laboratory at Pontifícia Universidade Católica do Rio de Janeiro (PUC-RIO). The room has an area of 4.5 x 4.5 meters, with an equipment bench and a locker against the side walls.

The minimum distance between transmitter and receiver to guarantee far field operation is 21.65 cm at 26.5 GHz and 32.67 cm for 40 GHz, obtained from:

$$D_{Far\ Field} = \frac{2 \cdot Dim^2}{\lambda} \tag{3.21}$$

where Dim is the largest antenna dimension, equal to 3.5 cm in our case, and λ is the wavelength. The penetration loss was obtained as the difference between the received power levels of the unobstructed path (LOS) and the received power level with the material obstructing the path between transmitter and receiver (NLOS) as illustrated in Figure 3.4.

(a)

(b)
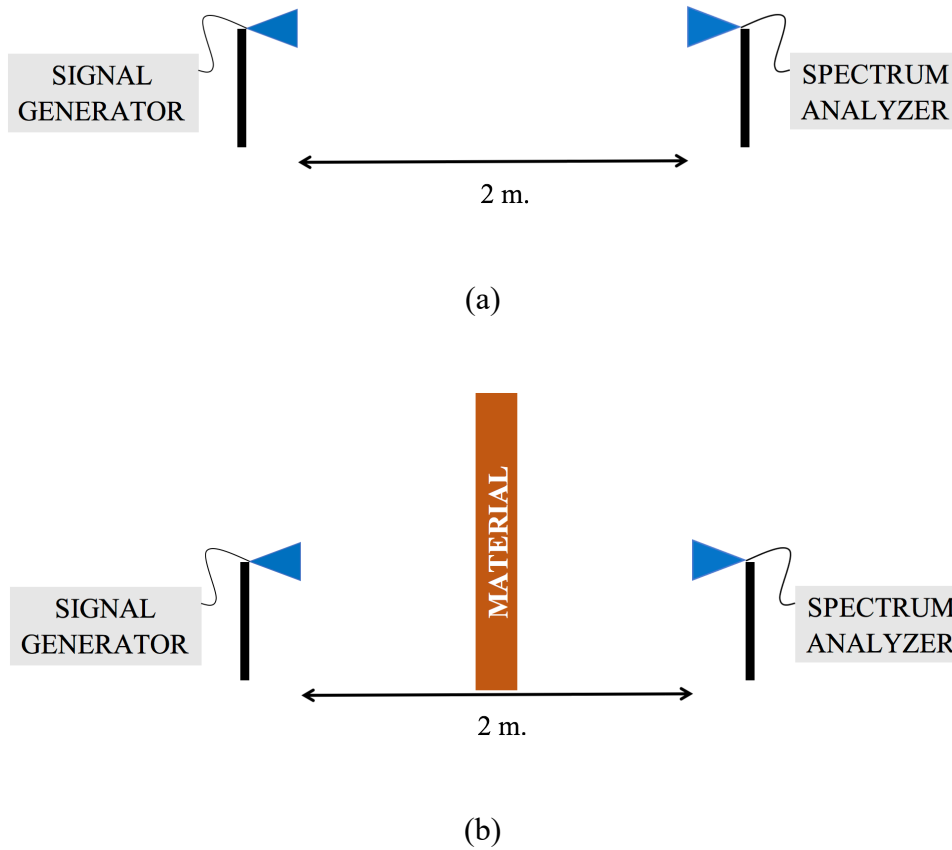
Figure 3.4: (a)Unobstructed link (LOS); (b) Obstructed Link (NLOS)

First, the received power without obstructions was measured at frequencies between 26.5 and 40 GHz, in steps of 250 MHz for each set of measurements to provide a reference baseline. A CW was transmitted with 0 dBm power level and each received power level was obtained as the average of 30 samples in the spectrum analyzer. The process was repeated 3 times and average value was taken as a final result for each frequency and each material. Then, the link was obstructed by each material and the NLOS received power was measured using the same procedure. The penetration loss was then calculated as the difference between the unobstructed and obstructed power level for each frequency.

A distance of 2 meters between transmitter and receiver was selected. At this distance, the antenna illuminates the material 30 cm horizontally and 32 cm vertically. The material was located at the center, between transmitter and receiver and the dimensions of the materials must be larger than 30 x 32 cm to reduce multipath. Characteristics of tested materials are described in Table 3.2.

Material	Width (cm)	Height (cm)	Thickness (cm)
Thin Polystyrene	50	100	1.2
Thick Polystyrene	50	100	4.9
Thin pressed wood	80	100	0.35
Thick pressed wood	92	205	1.6
Thin wood	76	129.5	0.8
Thick wood	79.7	209.5	3.5

Table 3.2: Tested Materials in first set of measurements

In the first set of measurements, negligible penetration loss was observed for thin and thick polystyrene. Pressed wood penetration loss has a strong relation with its thickness, varying from 0.5 dB to 2.9 dB for thin pressed wood and from 5.1 dB to 7.7 dB for thick pressed wood.

Solid wood penetration loss shows an increase with frequency higher frequencies. For thin wood, it increases from 4.4 dB at 26.5 GHz to 6.7 dB at 40 GHz. For thick wood, the measured variation is surprising large, from 3.4 dB at 26.5 GHz to 18.2 dB at 40 GHz. This effect must be investigated with additional measurements. All these results are illustrated in Figure 3.5.
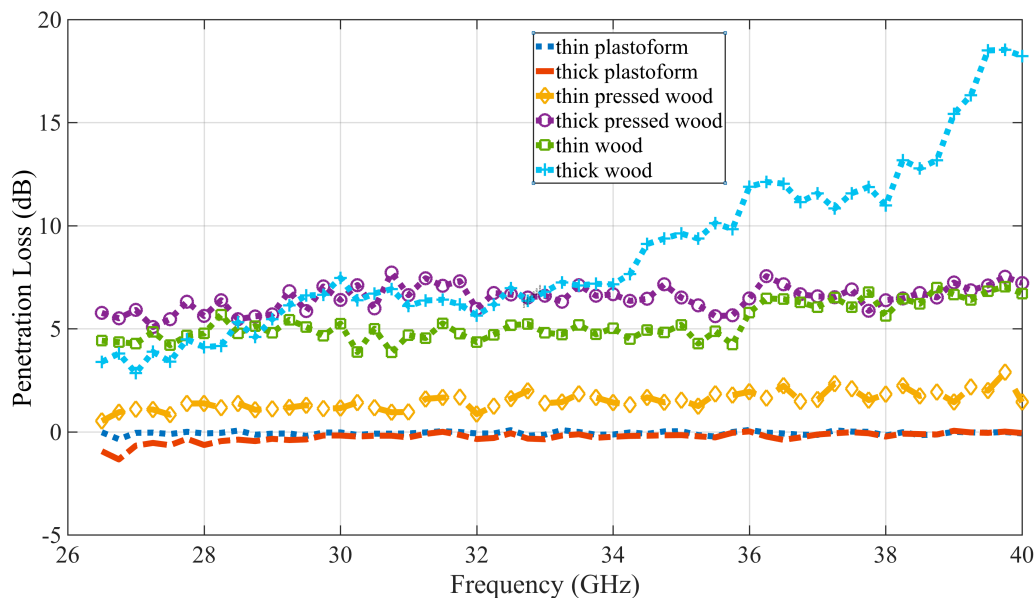
Figure 3.5: Measurement Results for the first set of measurements

To measure materials in a more usual environment, a second set of measurements was performed in a meeting room with large windows and a wide door which accessing a terrace. The measurement was made with the materials described in Table 3.3, and the results are presented in Figure 3.6.

Material	Width (cm)	Height (cm)	Thickness (cm)
Glass window	100	120	1
Brick wall	300	110	28
Wooden door (center)	150	200	5.8
Wooden door (side)	150	200	3.5

Table 3.3: Tested Materials in second set of measurements

In the second set of measurements the penetration loss for the glass window and the wooden door were approximately constant, except for small measurement errors. The average glass window penetration loss was 3.5 dB, varying from 1.5 dB to 5.5 dB. The wooden door was measured twice, at its center ($Door_C$) which has the higher thickness and at the door side, which has a lower thickness ($Door_L$). As in the case of the pressed wood, the wooden door presented a penetration loss increase with thickness. The average penetration loss for $Door_L$ was 14.4 dB and for $Door_C$ 24.85 dB. For the brick wall, the penetration loss shows values from 40 dB to 65 dB, increasing with frequency but with significant variations along the frequency range.
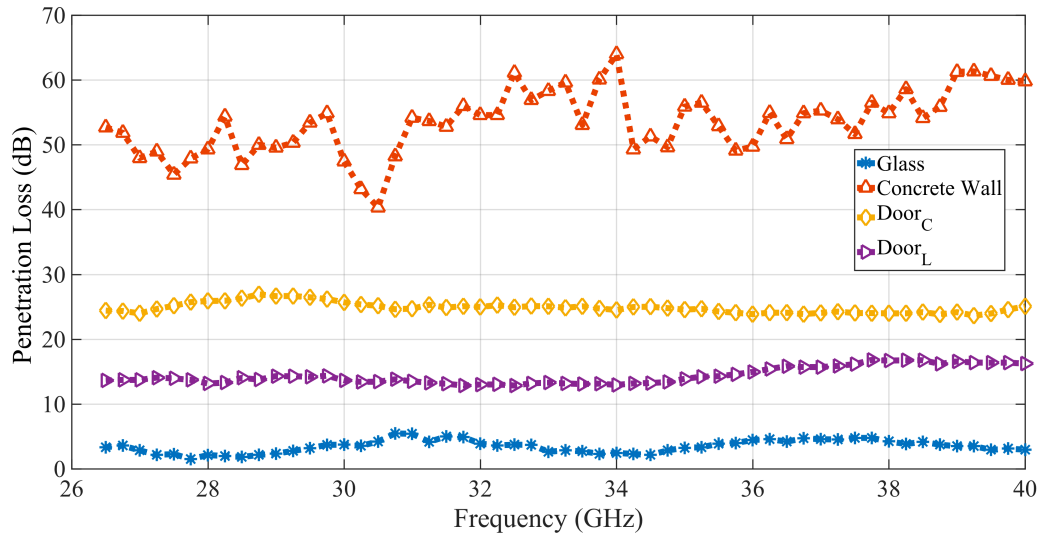
Figure 3.6: Measurement Results for the second set of measurements

Both measurement scenarios are shown in Figure 3.7, where the left photos show measurements in the laboratory and the right photos show measurements in the meeting room.

Figure 3.7: Scenario 1 (left photos) and Scenario 2 (right photos)

In Figure 3.5, it is possible to see a negative penetration loss for polystyrene in the lower range of frequencies tested. This corresponds to a gain instead of a penetration loss, which theoretically is not possible unless our environment has

intense multipath. Then, due to the lack of an large anechoic chamber, these measurements were repeated in different types of environments in order to define the environment with less multipath presence.

The meeting room, a balcony and an open terrace were the scenarios where new set of measurements were made. The meeting room has laminated wood floor with big windows around the room and a brick wall, it is totally ceiled. Balcony has a ceramic floor, no wall on right side and small thin wood wall on left side, it is totally ceiled. Terrace has a concrete floor; no close walls and it is an open environment. For other hand, to reduce even more the possibility of multipath presence, the distance for this new set of measurements was changed to just one meter between the transmitter and the receiver. At this distance, the antenna illuminates the material 15 cm horizontally and 16 cm vertically.

In Figure 3.5 the thick wood presented a different behavior than the other materials with a large variation in penetration loss while frequency increase. After some additional measurements, it was defined that this variation appears due to the metal door handle near to the illumination area of the antenna into the material (our thick wood, was actually a wooded door from one class laboratory, taken off to make this measurement). Then, this material was excluded for the third set of measurements. Table 3.2 and Figure 3.8 shows the characteristics of the three measurement scenarios.

Material	Width (cm)	Height (cm)	Thickness (cm)
Thin Polystyrene	50	100	1.2
Thick Polystyrene	50	100	4.9
Thin pressed wood	80	100	0.35
Thick pressed wood	92	205	1.6
Thin wood	76	129.5	0.8

Table 3.4: Tested Materials in the third set of measurements

Figure 3.8: Measurements scenarios: Balcony (up-left), Terrace (up-right), meeting room (bottom-left)

From [26], the penetration loss in polystyrene is expected to be negligible and this reference will be used as a principal factor to select the environment with less multipath presence. Results of this measurements are shown in Figure 3.9 (a-c) for the three scenarios: meeting room, balcony and terrace respectively.
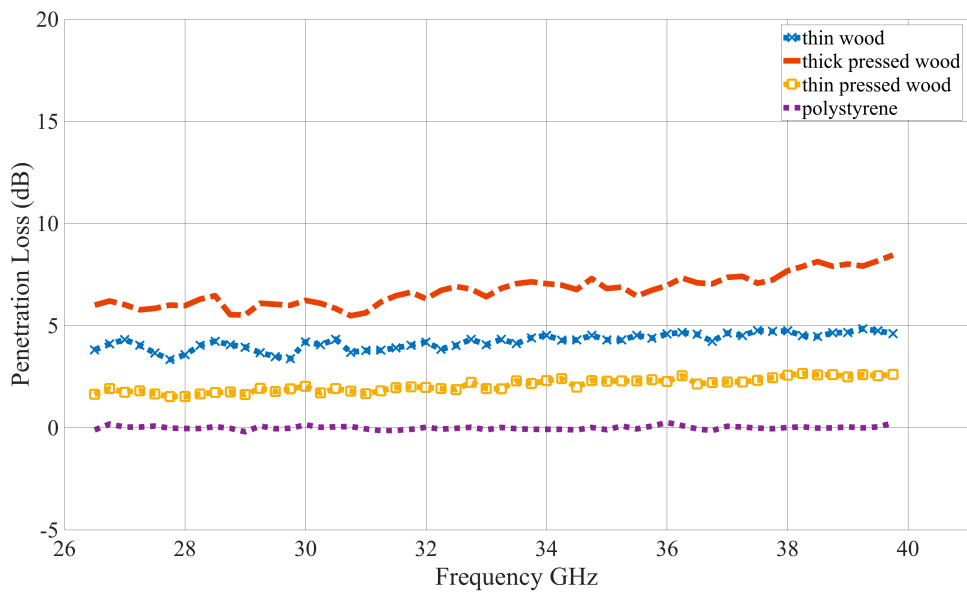
(a) Meeting room measurements
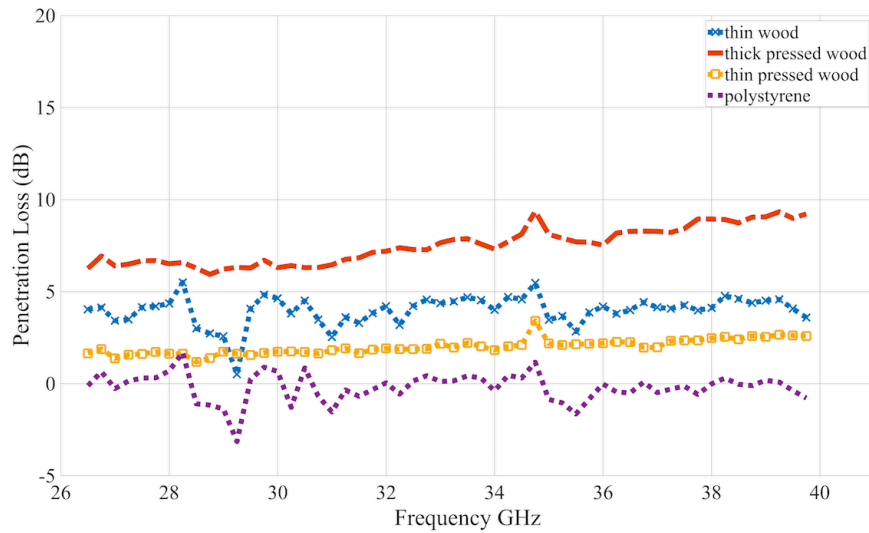
(b) Balcony measurements
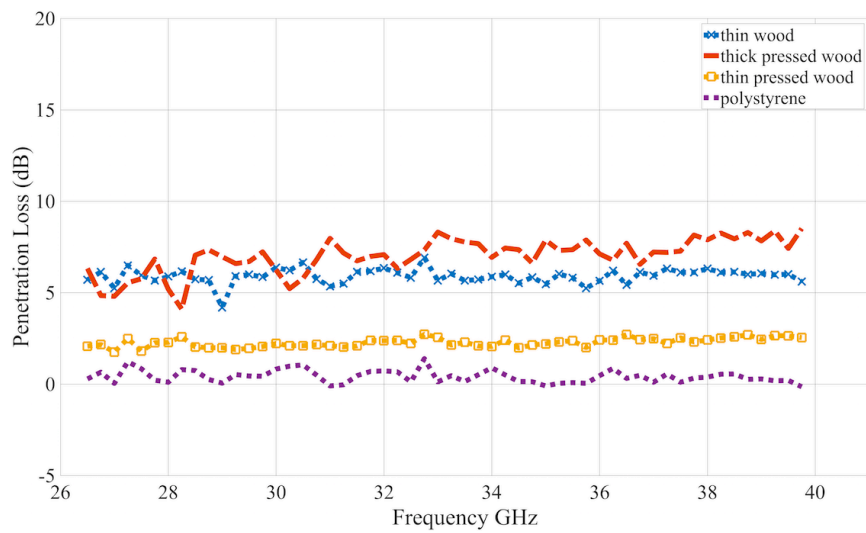
(c) Terrace measurements

Figure 3.9: Measurements Results

It was found that the polystyrene thickness does not affect in result measurements since similar results for thin and thick polystyrene were found in the three environments. Therefore, figures show measurement results for thick and thin polystyrene as they would be just one material.

Comparing the results from the 3 scenarios, it was found that meeting room is the environment with less multipath presence, and results obtained in that scenario were taken as final results. Average penetration loss for the whole range of frequencies are listed in Table 3.5 and compared with results from other references [22][26][27][28][29].

Material	Measured value [dB]	Other references [dB]
Polystyrene	0	0
Thin pressed wood	2.1	1.92
Thick pressed wood	6.7	8.8
Thin wood	4.2	3-5
Glass	3.5	3.6-3.9
Door$_L$	14.1	13.3
Wall	40-65	46-57

Table 3.5: Penetration Loss (dB) through Materials

3.4　Reflection Measurements

The measurement setup was the same used in measurements of penetration loss, with the transmission of a CW with 0 dBm power level by the signal generator and a 1-meter propagation distance. As shown in Figure 3.10, both antennas were positioned in front of the material and the received power measured. The antennas were positioned to achieve incidence and reflection angles from 15° to 45° in steps of 5°, varying the operation frequency from 26.5 GHz to 39.5 GHz in steps of 250 MHz. The received power was measured for each angle, each material and for each frequency.
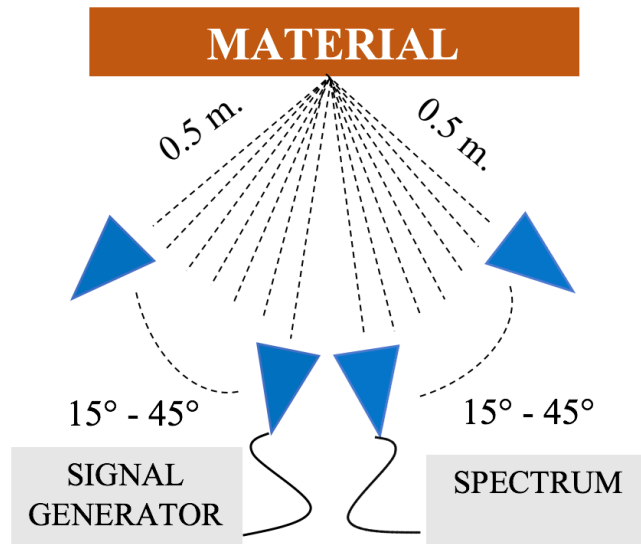
Figure 3.10: Measurements of Reflection through materials

The magnitude of the reflection coefficient $|\Gamma|$ can be calculated from [24]:

$$|\Gamma| = \frac{d_1 + d_2}{d_{LOS}} \sqrt{\frac{(P_R)_{refl}}{(P_R)_{LOS}}} \qquad (3.22)$$

where d_1 is the distance from transmitter to the material, d_2 is the distance from receiver to the material, d_{LOS} is the distance from transmitter to receiver in a LOS communication, $(P_R)_{refl}$ is the reflected received power level, $(P_R)_{LOS}$ is the LOS received power level. LOS received power level was already obtained from penetration loss measurements. Figures 3.11 and 3.12 shows the reflection coefficients for different construction materials for frequencies between 28 GHz and 38 GHz .
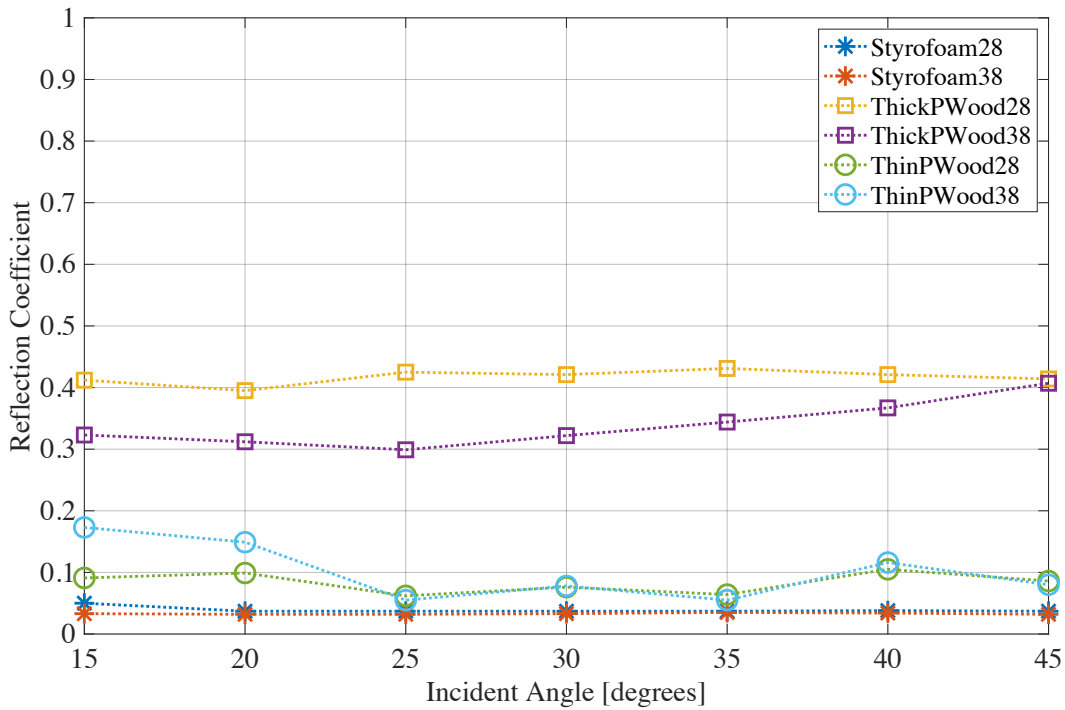
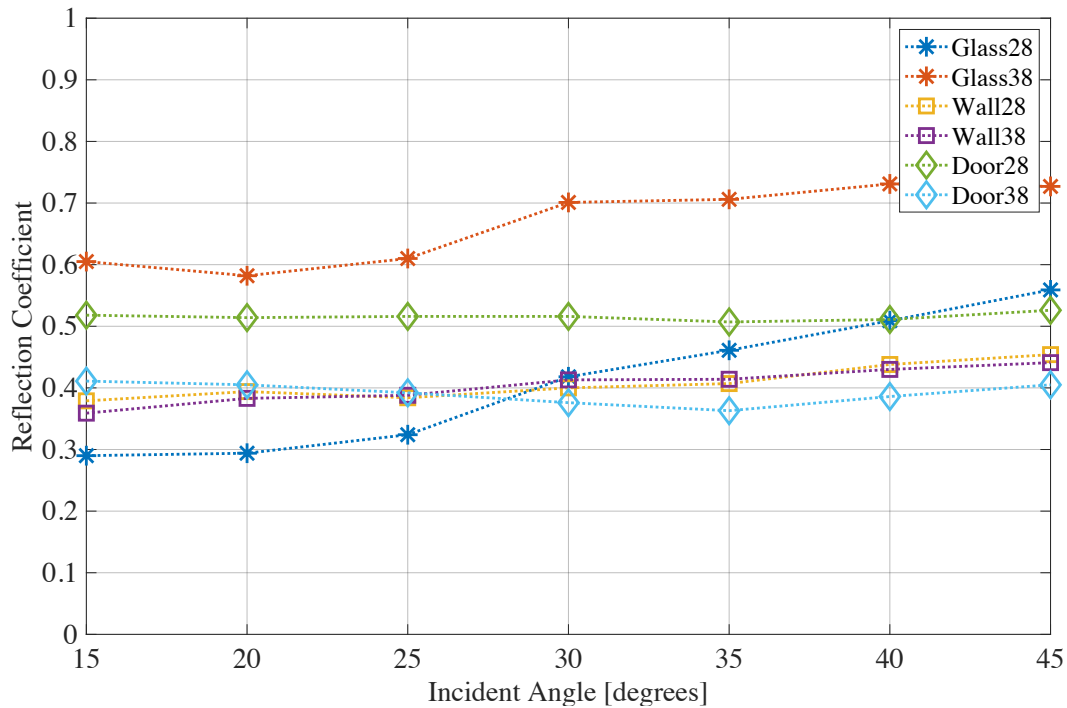**Figure 3.11:** Reflection Coefficients for 28 GHz and 38 GHz

Figure 3.12: Reflection Coefficients for 28 GHz and 38 GHz

Note that polystyrene and thin pressed wood have the lowest reflection coefficients, similarly to other researchers results. Both polystyrene and thin pressed wood has largest reflection coefficients for low incidence angles at 28 GHz. Thick pressed wood presents the largest reflection coefficient for incidence angles of 35º at 28 GHz and 45º at 38 GHz. Thick wood characteristics can be compared with wood results found by other works, where reflection coefficient values go around 0.45 [5]. In general, largest values were obtained at 38 GHz for incident angles from 15º to 45º.

The glass window has the largest reflection coefficient of all materials. A value of 0.559 was obtained with an incident angle of 45º at 28 GHz and 0.731 - 0.727 with 40º and 45º at 38 GHz, a reflection coefficient value of 0.7 was found in other researchers [24] . The wooden door presents the highest reflection coefficient at 45º in both frequencies, 0.526 for 28 GHz and 0.405 for 38 GHz, values are very comparable to results found in literature, around 0.51. Finally, brick wall present values from 0.379 to 0.454 at 28 GHz and from 0.359 to 0.441 at 38 GHz. In other research, where a wall was a little thicker, reflection coefficient goes around 0.6 [22][24].

4

Outdoor Measurements

4.1   Path Loss Prediction Models

Path loss prediction models are important to understand how the signal behaves in a certain environment These models are used for coverage predictions in the planning and designing cellular communications systems.

The most basic path loss model is the *Free Space Path Loss* (FSPL), which gives the path loss over air without obstructions. It gives a fast idea of the minimum path loss that the signal will have. There are also several single frequency and multi-frequency path loss models that considers the effect of topography and buildings in the region.

In the first group of single frequency models, the *floating intercept* (FI), also known as *alpha-beta* (AB), and the *close-in free space reference distance* (CI) are the most commonly used [30][31][32]. Some comparisons between both models can be found in [30][33][34]. The most common multi-frequency models used are *Alpha-Beta-Gamma* (ABG), an extension of the AB model, and the *close-in free space reference distance with frequency dependent path loss exponent* (CIF), which is an extension of the CI model.

4.1.1 Free Space Path Loss Model

The free space path loss model considers line-of-sight (LOS) path. There is not reflection or diffraction and it considers an ideal environment for propagation. Its equation is given by [5]:

$$FSPL(d)[dB] = 20log_{10}\left(\frac{4\pi d}{\lambda}\right) \qquad (4.1)$$

Since $\lambda = c/f$ we have:

$$FSPL(d)[dB] = 20log_{10}\left(\frac{4\pi df}{c}\right) \qquad (4.2)$$

where d is the distance between the transmitter and receiver, in meters, f is the frequency in Hz and c is the speed of light, $c = 3 \times 10^8\ m/s$. In millimeter waves frequencies will be in GHz and distances in meters, then, equation (4.2) becomes:

$$FSPL(d)[dB] = 32.45 + 20log_{10}(d[m]) + 20log_{10}(f\ [GHz]) \quad (4.3)$$

4.1.2 Alpha-Beta and Alpha-Beta-Gamma Models

The Alpha-Beta model is a simple method that use only two coefficients to predict path loss. It is given by [35][36][39]:

$$PL^{AB}[dB] = 10\alpha log_{10}(d) + \beta \qquad (4.4)$$

where, $PL^{AB}[dB]$ is the predicted path loss in decibels, α is the coefficient that characterize the dependece of the path loss with the distance d, which is the distance in meters between the transmitter and the receiver, β is a linear coefficient in dB.

The Alpha-Beta-Gama model [32][37]is an updated version of the AB model and it includes the path loss frequency dependence and a log-normally distributed variable corresponding to the large-scale fading. It is expressed as:

$$PL^{ABG}[dB] = 10\alpha log_{10}\left(\frac{d}{1\ m}\right) + \beta + 10\gamma log_{10}\left(\frac{f}{1\ GHz}\right) \qquad (4.5)$$

where, $PL^{ABG}[dB]$ is the predicted path loss in decibels, γ is the coefficient that shows the variation of the path loss with frequency f in GHz. If measurements are made in a single frequency, $\gamma = 0$, the ABG model will be equal to AB model.

4.1.3 CI and CIF models

The CI model is given by [31][38]:

$$PL^{CI}[dB] = PL_{FS}(f, d_0 = 1m)[dB] + 10n\log_{10}(d) + X_\sigma^{CI} \qquad (4.6)$$

where $d \geq d_0$ and $d_0 = 1$ meter and $PL_{FS}(f, d_0 = 1m)[dB]$ can be calculated with (4.3). Take in mind that CI model has an intrinsic frequency dependence with the term $PL_{FS}(f, d_0 = 1m)$ and has only one coefficient to be optimized which is the path loss exponent (PLE) n. CI model is applicable to both single and multi-frequency cases. For multi-frequency cases is used the CIF model, given by:

$$PL^{CIF}[dB] = PL_{FS}(f, d_0 = 1m)[dB] + 10n\log_{10}(d)$$
$$+ 10nb\left(\frac{f - f_0}{f_0}\right)\log_{10}(d) + X_\sigma^{CIF} \qquad (4.7)$$

where n represents the distance dependence of path loss, like in CI model, and b describe the linear frequency dependence of path loss. The parameter f_0 is a reference frequency that can be calculated by:

$$f_0 = \frac{\sum_{k=1}^{K} f_k N_k}{\sum_{k=1}^{K} N_k} \qquad (4.8)$$

where K is the number of frequencies used while the model is applied, N_k is the number of points that the kth frequency f_k has, and X_σ^{CIF} describes the large-scale shadowing.

Note, that the CIF model becomes the CI model when only one frequency is used, in that case, $f_0 = f$ or $b = 0$.

4.2 Measurements in the university campus

Using the signal generator, a CW at 0 dBm was transmitted from the last floor of the Leme building (LEM) in Pontifical Catholic University of Rio de Janeiro campus (PUC-RIO). The transmitter antenna was placed on a tripod at a

height of 1.5 meters above the floor, achieving a total height of 50 meter above ground and positioned in the middle of the edge to avoid shadowing. This imitated a typical sector antenna installation used in microcell deployments, where base station antennas are mounted on the external wall or edge of multistory buildings.

The area considered for measurements lies within the university campus with short distances between buildings, a large green area, a parking building and a construction area, as illustrated in Figure 4.1. The construction area is shaded in yellow and there is a metallic crane stationed in the middle of this area.
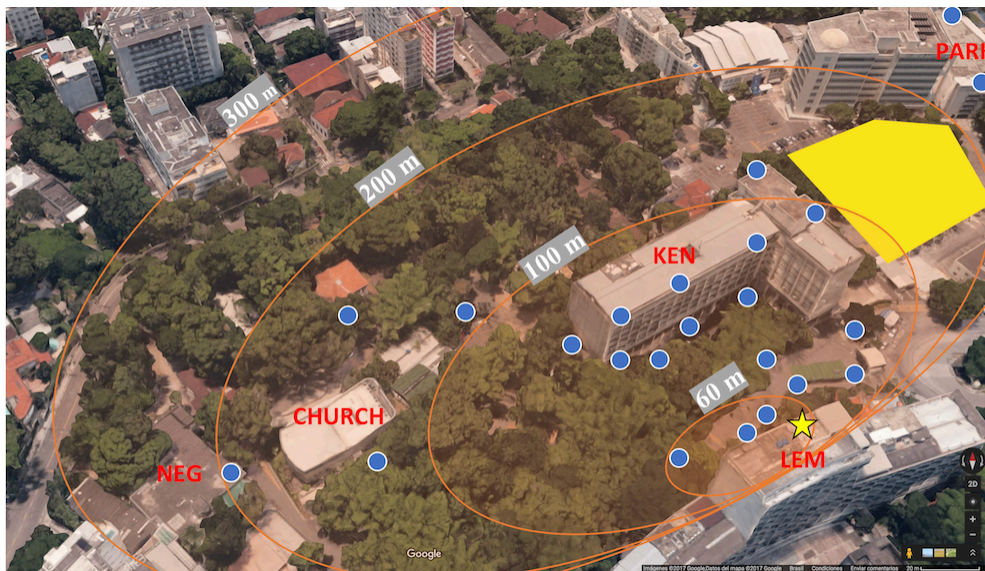

Figure 4.1: Outdoor Measurements Scenario, PUC-RIO

Receivers were positioned at several points points of the campus and at more distant points where energy was available. The 23 receiver points where selected to cover approximately 50% of the total campus area. Three receivers were located inside class rooms and the received power levels measured with the windows opened. The height of these class rooms above ground was 32 meters. Two other receiver points where positioned in Kennedy Building's (KEN) rooftop at a height of 40 meters above ground. Finally, two receivers where positioned in the parking building (PARK) roof with 20 meters above ground and one receiver was positioned on Business School (NEG) roof with an elevation of 15 meters. All receiver points were within 300 meters of distance from the transmitter. In Figure

4.1, each receiver point is marked with a circular dot and transmitter with a yellow star.

Two Bosch GRL 825 laser distance measures were used to align the transmitter and the receiver antennas. Distances between transmitter and receiver varied from 54 meters to 271 meters and elevation angles from 8 degrees to 66 degrees, as shown in Table 4.1. Some paths were partially obstructed by foliage.

RX Point	Distance (m)	Elevation angle (º)	RX Point	Distance (m)	Elevation angle (º)
RX1	88,1	34	RX13	115,8	24
RX2	80.8	38	RX14	184.6	15
RX3	73,2	43	RX15	159,1	16
RX4	82,8	36	RX16	126,5	23
RX5	98,8	30	RX17	65,8	19
RX6	97,8	32	RX18	66,1	18
RX7	83,5	40	RX19	83,8	14
RX8	72,8	46	RX20	106,1	8
RX9	75,9	44	RX21	94,8	9
RX10	60	61	RX22	271	9
RX11	55,2	66	RX23	234,7	10
RX12	54,3	60			

Table 4.1: Receiver Distances and Elevation angles

Received power levels were measured with a signal analyzer and the maximum path loss at the receiver threshold was 140 dB. At each receiver point, the measurements were repeated 3 times and the results averaged. This process was repeated for each frequency between 27 and 40 GHz, in 1 GHz steps, at the same receiver points.

This process was repeated for each frequency with the same set of receiver points. Figure 4.2 and Figure 4.3 present results of measurements for 27 GHz and 40 GHz. Receiver points with a path loss lower than 120 dB are marked with the green color and a circular dot. A yellow triangle is used if path loss was between 120 dB and 140 dB, considered as a weak signal receiver point. At 27 GHz only

one receiving point has a weak signal, which represents 4.4% of the total receiver points. At 40 GHz, 26% of the receiveing points have a weak signal.

At RX13, close to the Church, the link is obstructed by foliage. This explain the weak signal in both frequencies at this receiver point. At 40 GHz, there are five additional receiver points with weak signal, including RX3 and RX15 that are less than 200 meters distance from the transmitter. This weak signal was caused principally because links at these points were partially obstructed by foliage. RX22, RX23 and RX 14 presented a weak signal at 40 GHz mainly due to the larger distance. These five receiver points do not present weak signal at 27 GHz as the free space loss at this frequency is significantly lower than at 40 GHz.
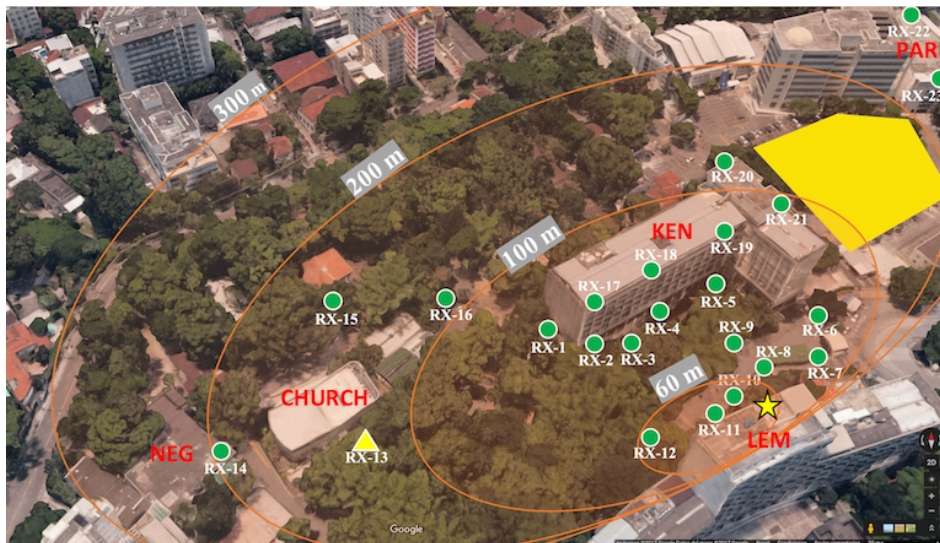

Figure 4.2: Measurements Results at 27 GHz. Green dots represent receiver points with a path loss lower than 120 dB and yellow triangles represent a receiver point with a weak signal (120 dB to 140 dB path loss). 4.4% of links have weak signal.

Figure 4.3: Measurements Results at 40 GHz. Green dots represent receiver points with a path loss lower than 120 dB and yellow triangles represent a receiver point with a weak signal (120 dB to 140 dB path loss). 26% of links have weak signal.

The measured path loss (PL) from transmitter to receiver is given by:

$$PL = P_{TX} + G_{TX} + G_{RX} - P_{RX} \tag{4.9}$$

were P_{TX} is the transmitted power in dBm, G_{TX} and G_{RX} are the transmission and reception antenna gains in dBi and P_{RX} is the received power level measured.

The path loss exponent n is a parameter that describes the dependence of the attenuation with the distance. It can be calculated by (4.6). Path loss exponent, $n = 2$, denotes free space propagation [7]. Figure 4.4 and Figure 4.5 show scatter plots of all measured path loss values versus distance for 27 GHz and 40 GHz. At 27 GHz we can see that majority of receiver points have a path loss exponent between n=2.35 and n=2.65. Only RX13 have a larger value of n=2.95. This is due to the presence of foliage in the TX-RX link. At 40 GHz path loss exponent values goes from n=2.20 to n=2.55 for majority of receiver points. The exceptions are n=2.90 for RX13 and n=3.5 for RX3. RX3 is a link with some foliage in the middle, explaining a higher path loss exponent value.
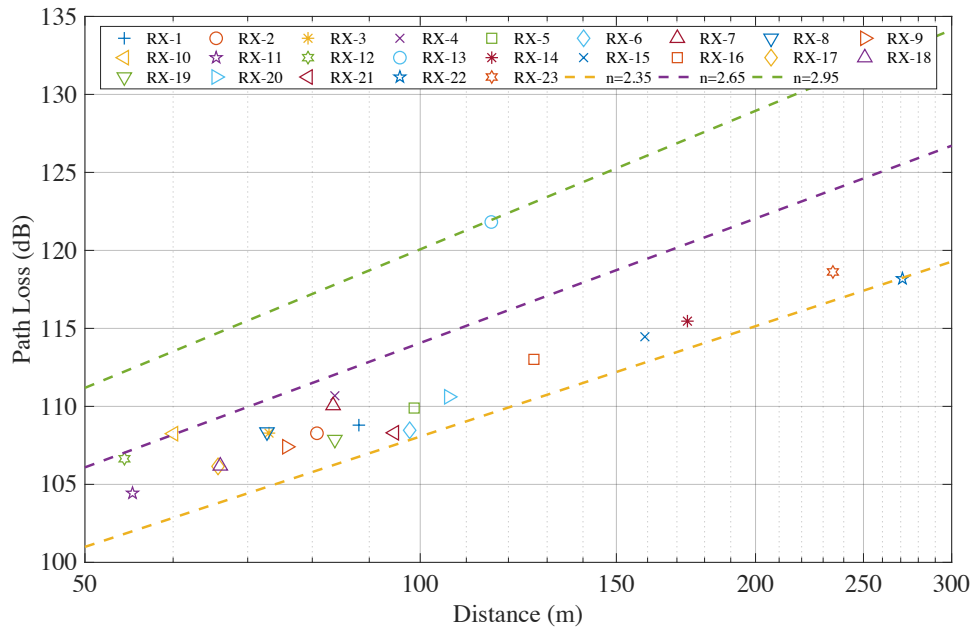
Figure 4.4: Scatter plot of path loss vs distance for measurements in 23 receiver points at 27 GHz in PUC-Rio campus during October (spring)
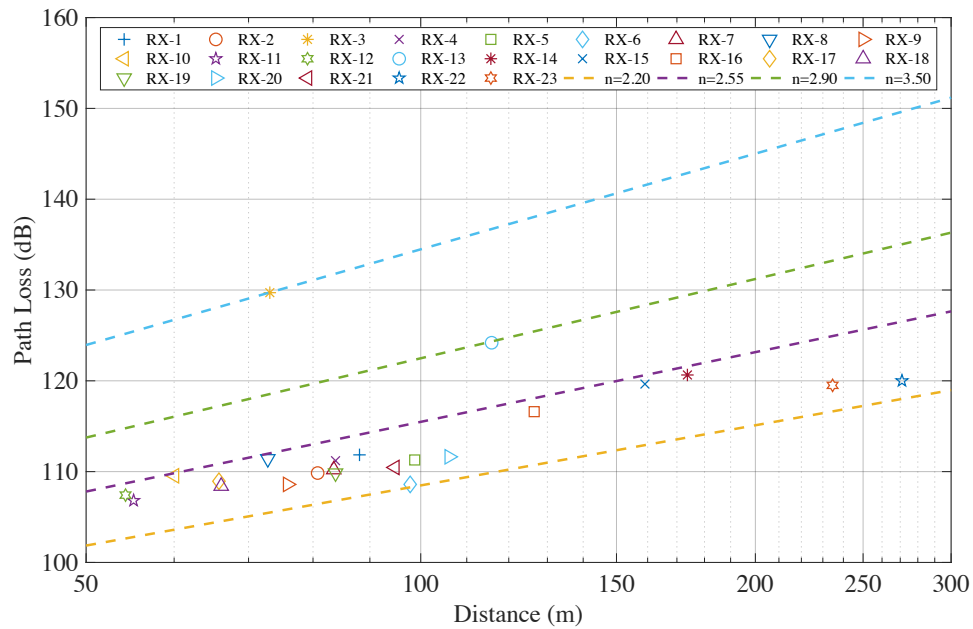

Figure 4.5: Scatter plot of path loss vs distance for measurements in 23 receiver points at 40 GHz in PUC-Rio campus during October (spring)

A comparison was made between the measured values and the three prediction models FSLP, CI and AB, for each frequency. Some results are shown in Figures 4.6 to 4.8.
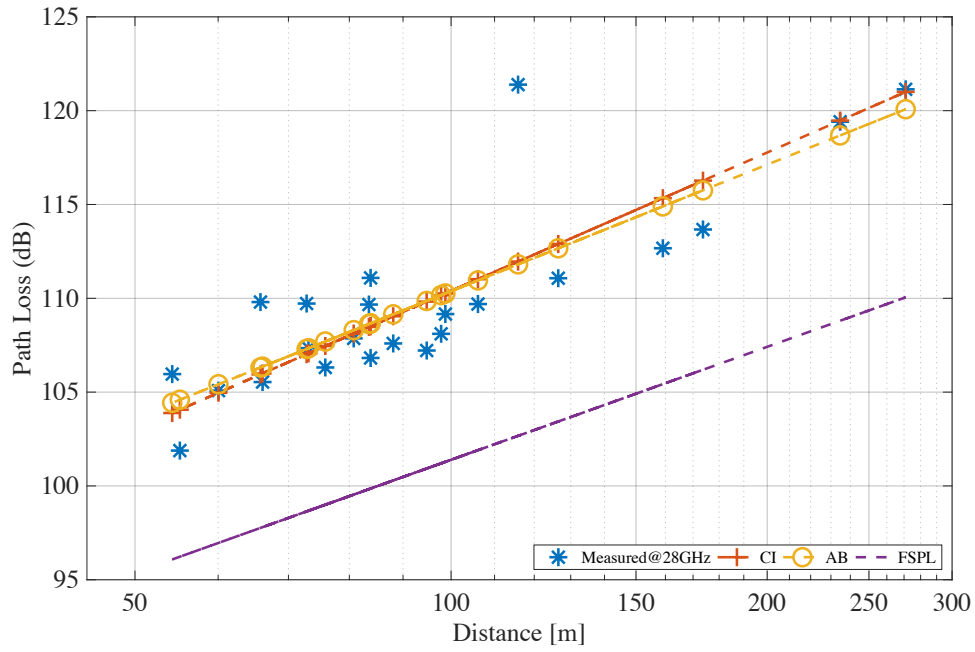
Figure 4.6: Comparison between path loss models with 23 receiver points considered at 28 GHz and with $n = 2.45$; $\alpha = 2.24$; $\beta = 65.6$
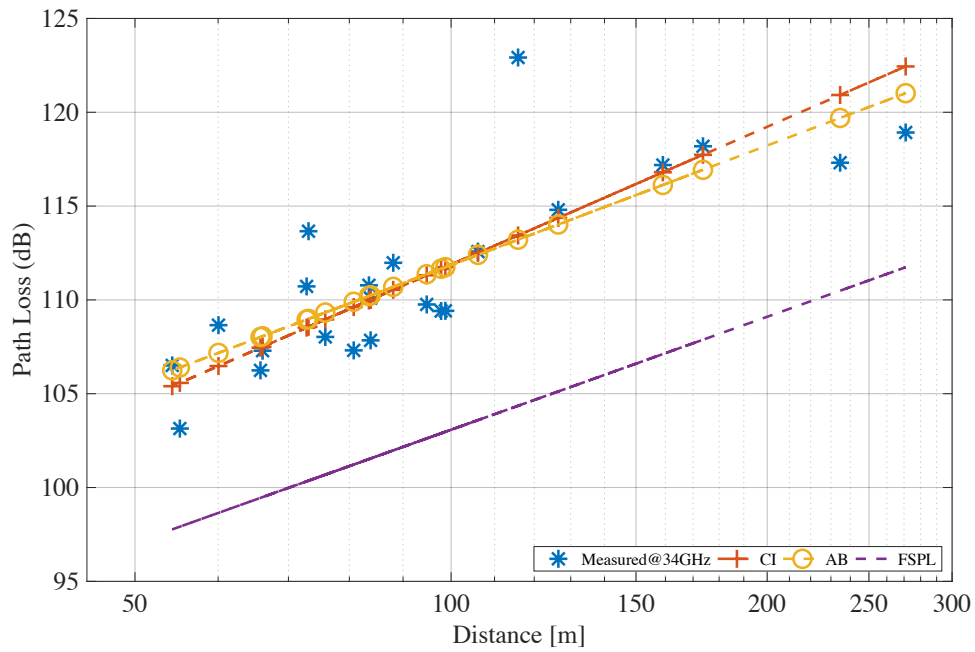

Figure 4.7: Comparison between path loss models with 23 receiver points considered at 34 GHz and with $n = 2.44$; $\alpha = 2.12$; $\beta = 69.6$
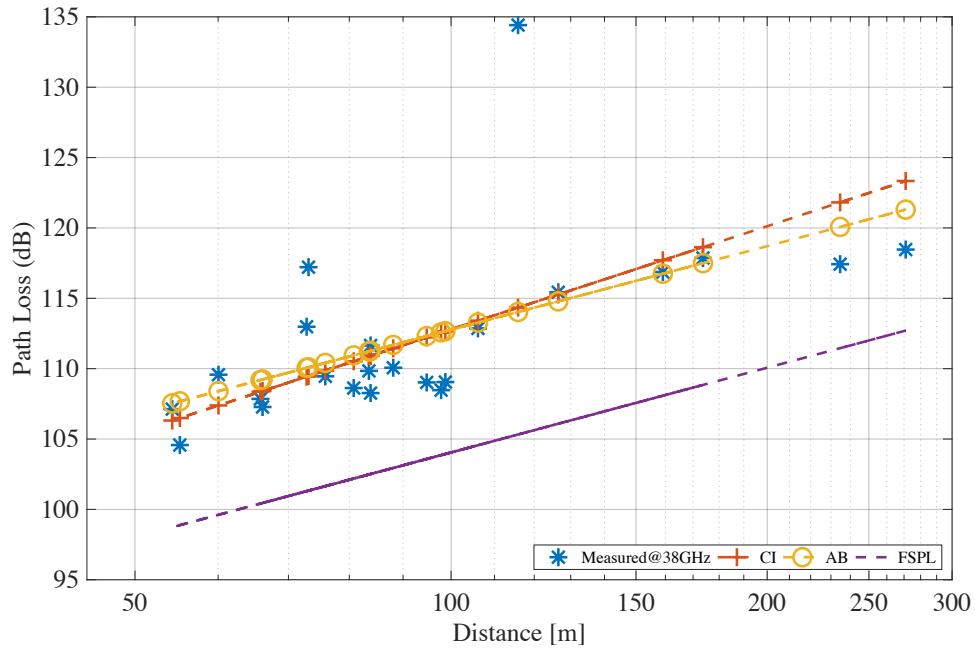
Figure 4.8: Comparison between path loss models with 23 receiver points considered at 38 GHz and with $n = 2.44$; $\alpha = 1.97$; $\beta = 73.4$

There are some points partially obstructed with foliage, such as RX1, RX2, RX4, RX10, RX16 and two receiver points fully obstructed by foliage, RX3 and RX13. It can be observed in Figures 4.6 to 4.8 that measured values for fully obstructed links depart significantly from predicted values by both models. These both receiver points were removed from the data set and path loss models were applied again. Results are shown in figures 4.9 to 4.11.

Figure 4.9: Comparison between path loss models with 21 receiver points considered (fully obstructed links were removed) at 28 GHz with $n = 2.43$; $\alpha = 2.13$; $\beta = 67.3$

Figure 4.10: Comparison between path loss models with 21 receiver points considered (Fully obstructed links were removed) at 34 GHz with $n = 2.41$; $\alpha = 2.08$; $\beta = 69.6$
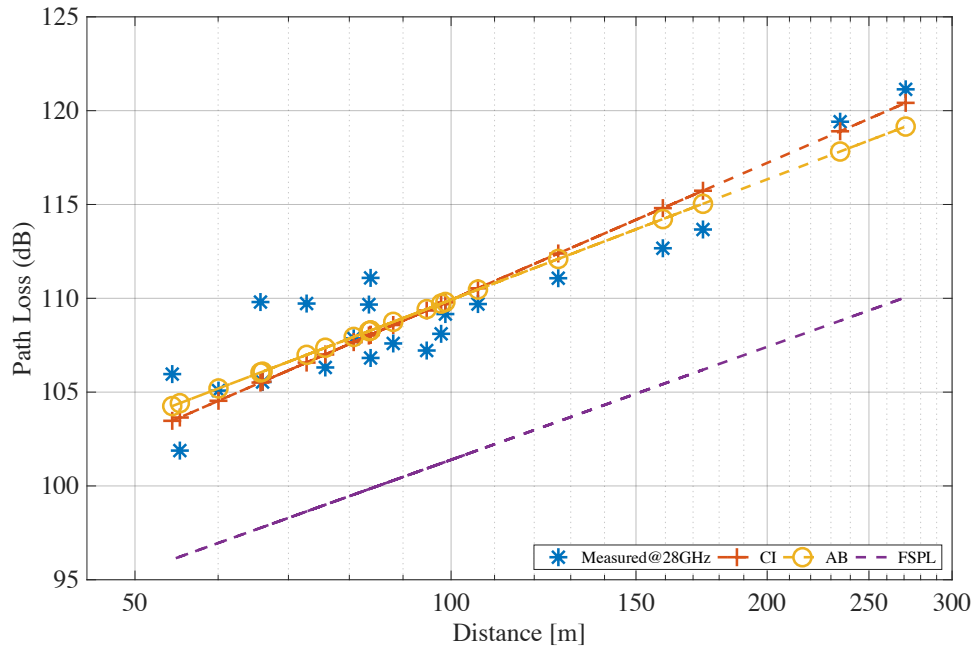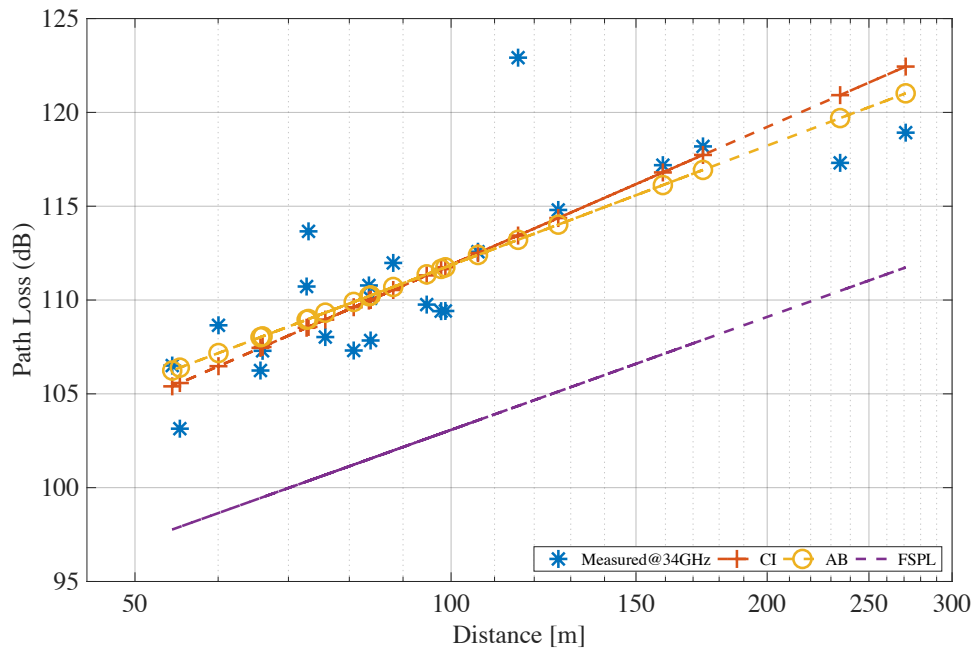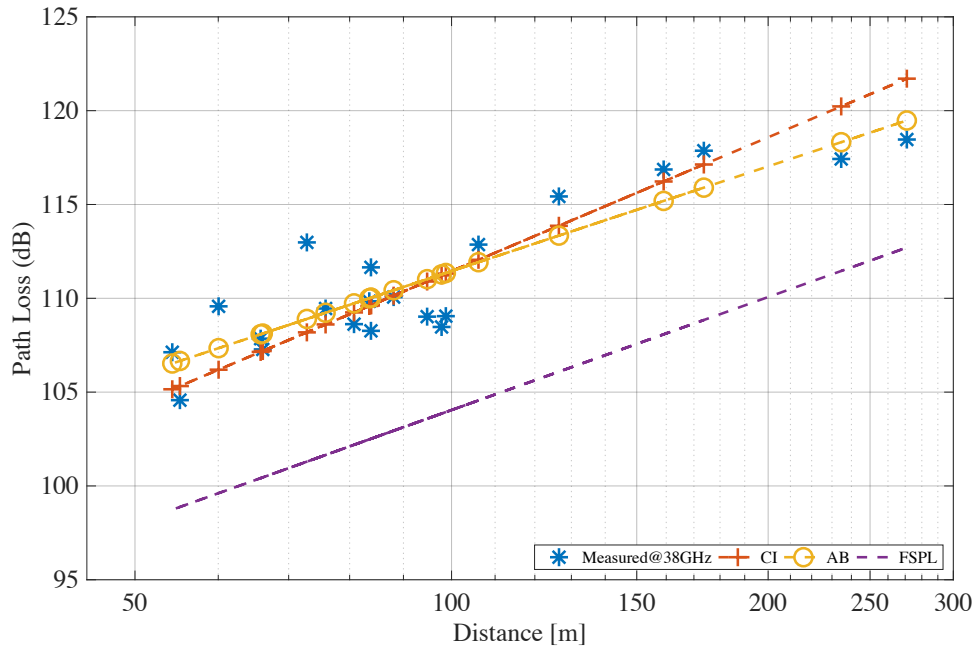
Figure 4.11: Comparison between path loss models with 21 receiver points considered (Fully obstructed links were removed) at 38 GHz with $n = 2.37$; $\alpha = 1.86$; $\beta = 74.4$

Table 4.2 shows the root mean square error (RMSE) values for both cases, considering path loss models CI and AB. As expected, path loss models adjust better when fully obstructed links are removed.

| Frequency GHz	RMSE			
	CI (23 points)	AB (23 points)	CI (21 points)	AB (21 points)
27	2,45	2,30	1,46	1,05
28	2,69	2,66	1,86	1,77
29	4,39	3,95	3,77	3,12
30	3,11	2,85	2,59	2,19
31	4,46	4,25	3,55	3,25
32	4,75	4,69	2,41	2,18
33	4,81	4,73	2,66	2,46
34	2,85	2,79	1,70	1,58
35	4,13	4,00	3,14	2,99
36	3,11	2,98	2,31	2,13
37	3,42	3,36	1,87	1,79
38	5,04	4,97	2,01	1,76
39	5,08	5,02	1,71	1,55
40	4,88	4,78	1,70	1,62

Table 4.2: Root Mean Square Error (RMSE) for CI and AB path loss models

If we consider the whole range of frequencies, the path loss models to considered are CIF and ABG. Since it was already seen that fully obstructed links deviate from the path loss models, only 21 receiver points were considered to adjust the models coefficients. Considering the regression results, equations (4.5) and (4.7) can be rewritten as:

$$PL^{ABG}[dB] = 19.2log_{10}\left(\frac{d}{1\ m}\right) + 67.9 + 3.56log_{10}\left(\frac{f}{1\ GHz}\right) \quad (4.10)$$

$$PL^{CIF}[dB] = PL_{FS}(f, d_0 = 1m)[dB] + 24.4log_{10}(d)$$
$$- 3.63\left(\frac{f - 32.5}{32.5}\right)log_{10}(d) \quad (4.11)$$

The path loss of the 21 receiver points in all frequencies are plotted in Figure 4.12 together with the adjusted ABG and CIF models were applied. The RMSE values obtained are 2.38 and 2.58 respectively. Both analysis indicate that the AB/ABG models give lower RMSE values.
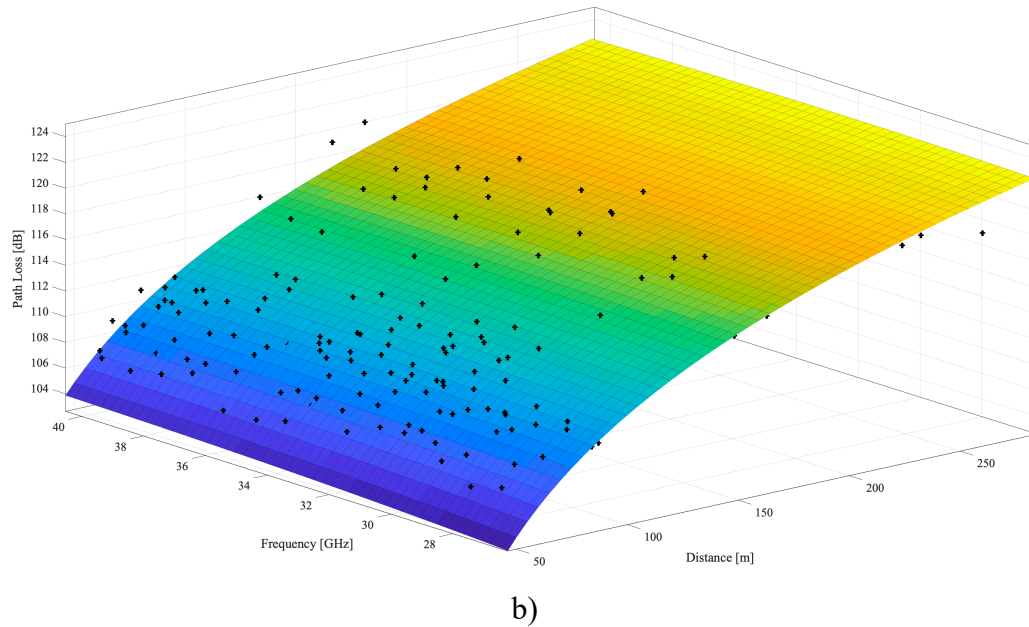

a)

b)
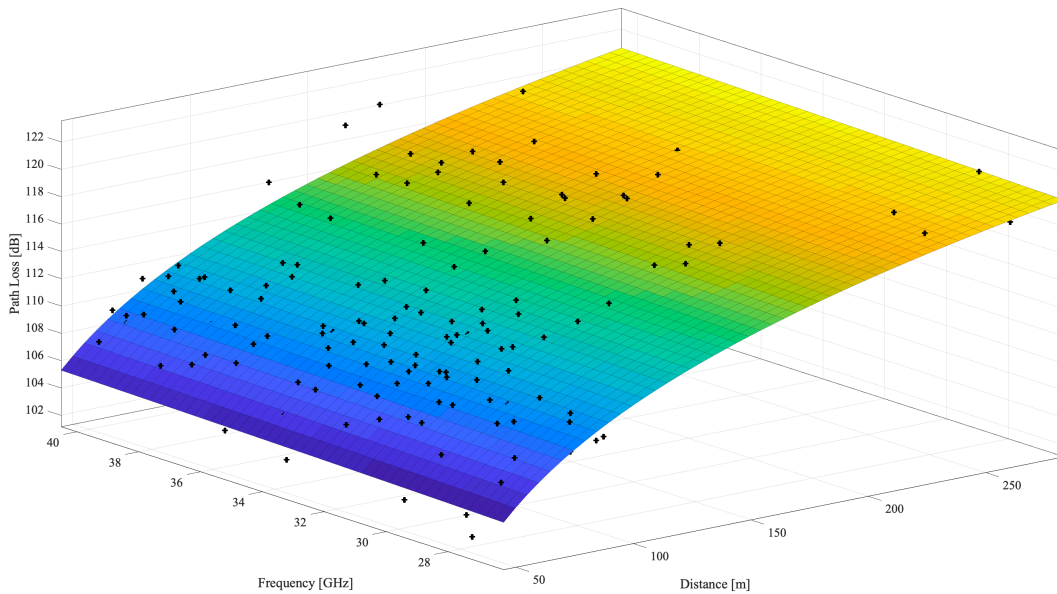
Figure 4.12: a) ABG path los model b) CIF path loss model

4.3 Effect of the relative height between Tx and Rx

One could expect that higher antenna heights results in lower path losses, as less obstruction will exist. In our measurements, three pairs of receiver points were positioned in same location in the campus but with different heights. Figure 4.13 shows path loss values of these pairs of points. Unfilled markers represent the lower receiver points and higher (additional 28 meters) receiver points are represented by filled markers. As expected, receiver points with less obstruction show lower path loss values.

Analyzing our measurement results, it is clear that the path loss has a dependence with frequency and distance. From Figure 4.13 it can be seen a dependence with antenna heights also exists. The dependence of path loss with these parameters can be observed in Figures 4.14 to 4.16. Partial obstruction by foliage can explain irregularities at some points.
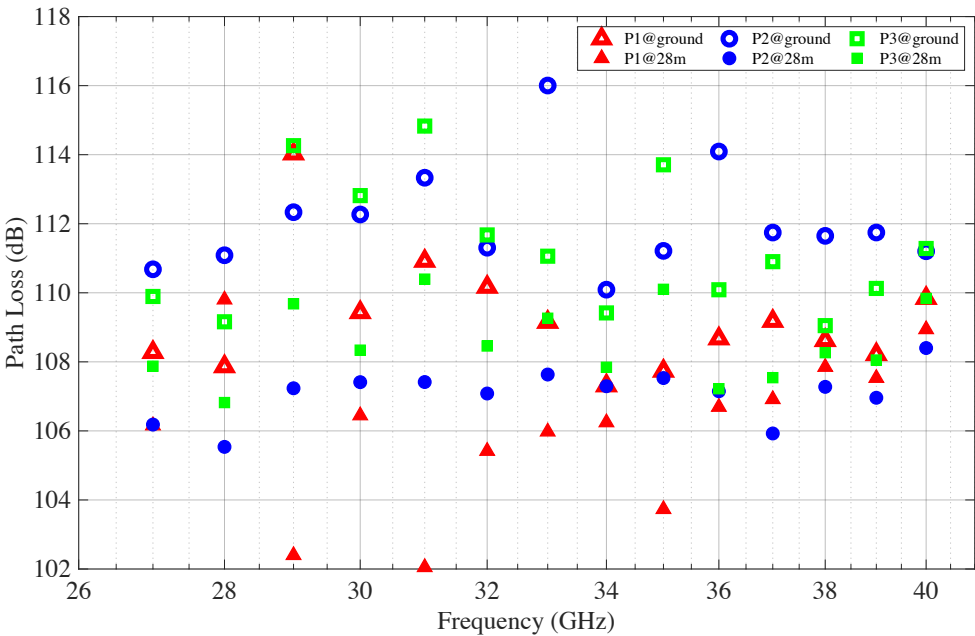
Figure 4.13: Scatter plot of path loss vs frequency for receiver points with same geographic location (same type of marker, unfilled and filled) but different antenna height.
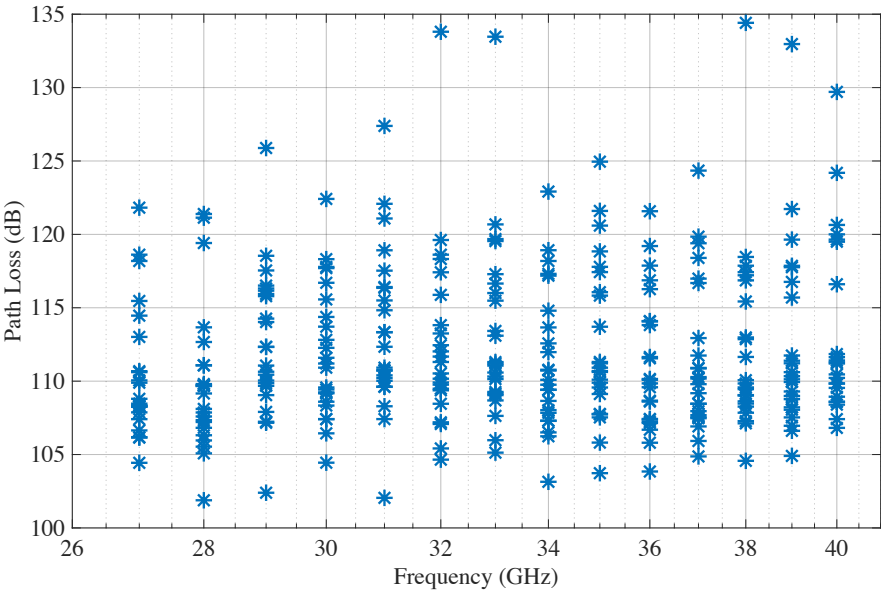
Figure 4.14: Path loss dependence on frequency
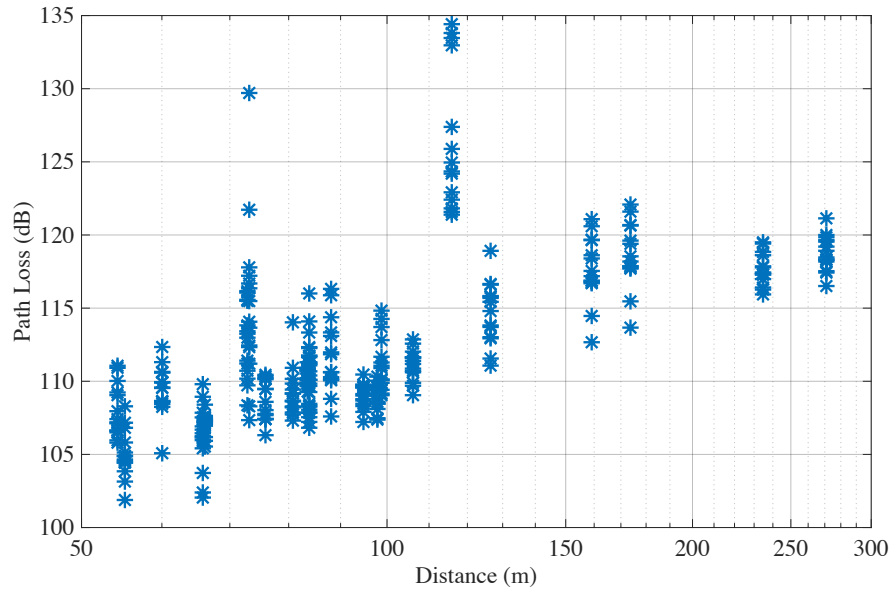
Figure 4.15: Path loss dependence on distance

Figure 4.16: Path loss dependence on Δh

From figure 4.16 we can see that the path loss increases as Δh increases. The models previously do not include this parameter in their predictions, so we propose a path loss model including the height difference between Tx and Rx. The height difference between Tx and Rx for all receiver points is shown in Table 4.3.

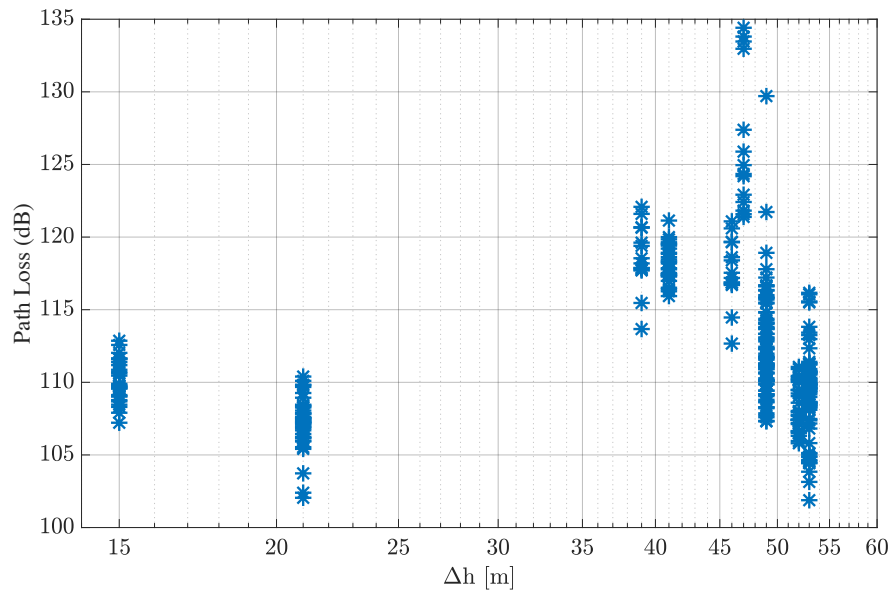| RX Point	Δh (m)	RX Point	Δh (m)
RX1	49	RX13	47
RX2	49	RX14	39
RX3	49	RX15	46
RX4	49	RX16	49
RX5	49	RX17	21
RX6	53	RX18	21
RX7	53	RX19	21
RX8	53	RX20	15
RX9	52	RX21	15
RX10	53	RX22	41
RX11	53	RX23	41
RX12	52		

Table 4.3: Height difference between Tx and Rx (Δh)

The proposed model is given by:

$$PL^{Prop}[dB] = 60.62 + 23.74 log_{10}(d) + 3.56 log_{10}(f) \\ + 4.54 log_{10}(\Delta h/d) \tag{4.12}$$

where d is the distance between transmitter and receiver in meters, f is the frequency in GHz and Δh is the relative height between transmitter and receiver in meters. A scatterplot of the measured and predicted values of path loss is shown in Figure 4.17.
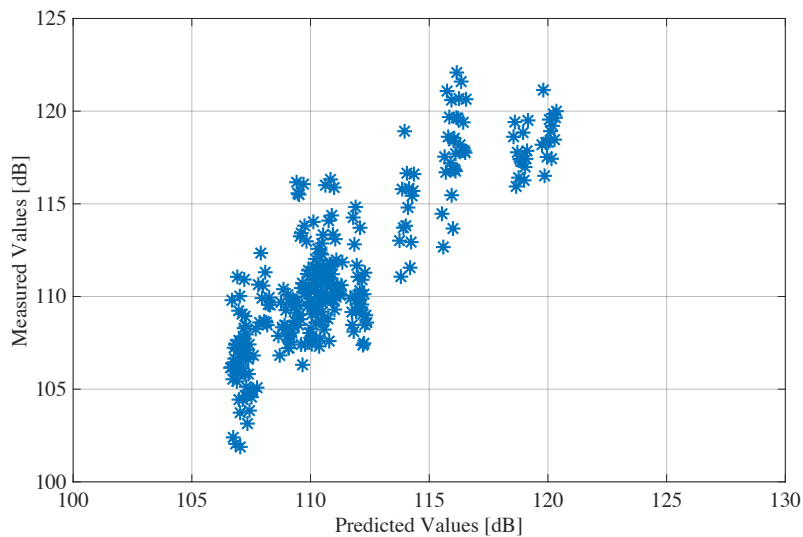
Figure 4.17: Path loss measured and predicted values.

The RMSE obtained with the proposed model is 2.21, which is lower than the values obtained with the ABG (2.38) and CIF (2.58) models.

4.4   Foliage Obstruction Analysis

As it was seen in the previous topics, vegetation produced higher path loss and needs to be considered in millimeter wave links. From the 23 receiver points measured, six links have partial and total foliage obstruction. Among them, RX1, RX2, RX4, RX10, RX16 have partial obstruction and RX3 and RX13 have total obstruction caused by foliage as illustrated in Table 4.4.

RX Point	View to Tx	Description
RX1		**Vegetation Depth:** **6.36 meters** **Vegetation type:** **Flamboyant – Mangueira – Bamboo** **Rx elevation angle:** **34 degrees**
RX2		**Vegetation Depth:** **2.57 meters** **Vegetation type:** **Palmeira** **Rx elevation angle:** **38 degrees**

RX3		**Vegetation Depth:** **13.54 meters** **Vegetation type:** **Palmeira-Mangueira** **Rx elevation angle:** **43 degrees**
RX4		**Vegetation Depth:** **1.16 meters** **Vegetation type:** **Mangueira** **Rx elevation angle:** **36 degrees**
RX10		**Vegetation Depth:** **1.23 meters** **Vegetation type:** **Pinheiro da mata** **Rx elevation angle:** **61 degrees**

RX13		**Vegetation Depth:** **28.09 meters** **Vegetation type:** **Mangueira** **Rx elevation angle:** **24 degrees**
RX16		**Vegetation Depth:** **2.24 meters** **Vegetation type:** **Mangueira** **Rx elevation angle:** **24 degrees**

Table 4.4: Illustration of links partially or totally obstructed by foliage.

To determinate the vegetation depth, the height of the threes along the link measured and the length of obstruction derived. Figure 4.18 shows the results for one of the links as an example. The solid line represents the direct link between Rx and Tx and dots represent the vegetation height [m] along this specific link. calculating the portion of the direct link that is blocked by vegetation, we find the vegetation depth, vd.
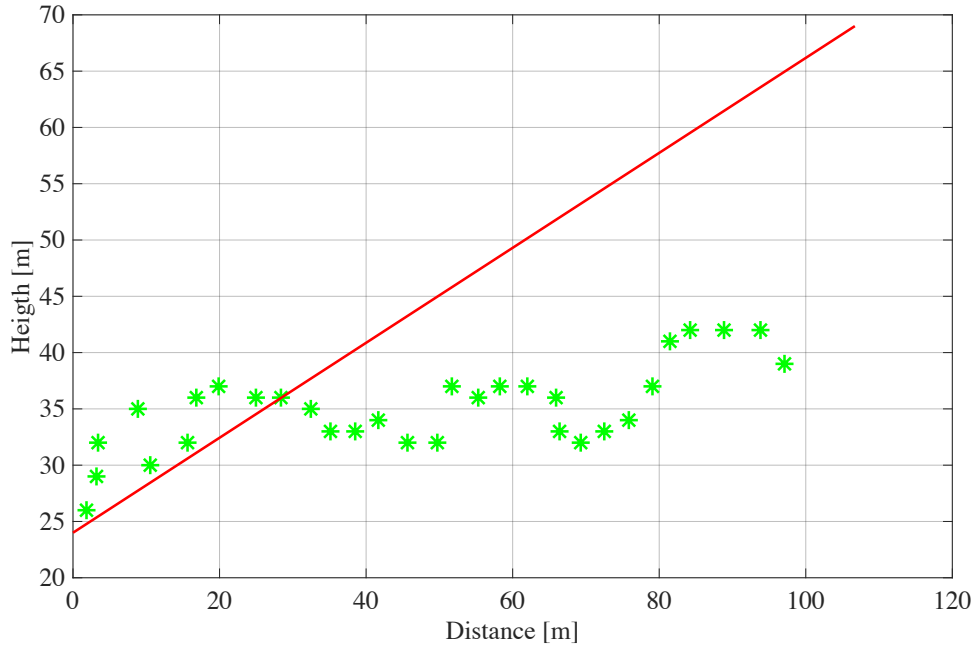
Figure 4.18: Vegetation depth for RX13

A prediction model is proposed that, besides including the relative height between Tx and Rx, also considers the vegetation depth in each link. The model is given by:

$$PL^{Prop}[dB] = 53.68 + 23.23log_{10}(d) + 8.39log_{10}(f)$$
$$+ 3.67log_{10}(\Delta h/d) + 0.47vd$$

(4.13)

where d is the distance between transmitter and receiver in meters, f is the frequency in GHz and Δh is the relative height between transmitter and receiver in meters and vd is the vegetation depth. A scatterplot of the measured and predicted values of path loss is shown in Figure 4.19. The RMSE obtained with the proposed model is 2.59 which is lower than the values obtained with the conventional models ABG (4.06) and CIF (4.16). Table 4.5 summarize the results obtained for both cases, considering or not the fully obstructed receiver points.
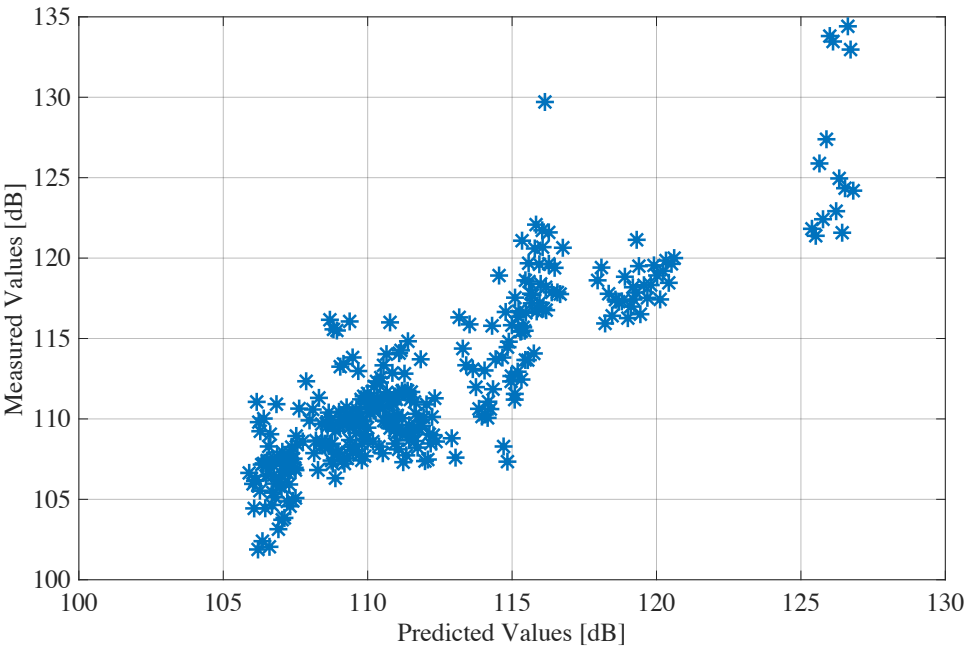
Figure 4.19: Path loss measured and predicted values, considering all receiver points

Nº of RX	ABG	CIF	Proposed model
21	2.39	2.58	2.21
23	4.06	4.16	2.59

Table 4.5: RMSE comparison between models for 21 receiver points (two fully obstructed links by foliage were excluded) and for 23 receiver points (without exclusions).

5

Indoor Measurements

5.1   Introduction

Indoor measurements are important to be able to estimate system coverage and capacity, as well as the overall network performance. Indoor wireless services are currently offered in 2.4 GHz, 5 GHz and 60 GHz (WiGig). Since future cellular systems will operate at frequencies in bands from 28 to 38 GHz, it is necessary to study the attenuation at these frequency band in indoor environments.

Our first set of measurements were conducted at the Center for Telecommunication Studies in PUC-Rio (CETUC), a department with many offices, classrooms and laboratories. A second set of measurements was performed in a long corridor in the Leme building. The range of frequencies used is 26.5 GHz - 40 GHz.

5.2   Indoor measurements in CETUC

Five positions for transmitters were selected in order to give full coverage to the offices and laboratories. As observed in Figure 5.1, TX1 (red star with green contour) enables communication with 9 RX points (green), TX2 (red star with blue contour) enables communication with 6 RX points (blue), TX3 (red star with orange contour) enables communication with 8 RX points (orange), TX4 (red star with purple contour) enables communication with 7 RX points (purple), TX5 (red star with yellow contour) enables communication with 7 RX points (yellow) and TX6 (red star with black contour) enables communication with 3 RX points (black). In total, 40 receiver points and 6 transmitter points were used.
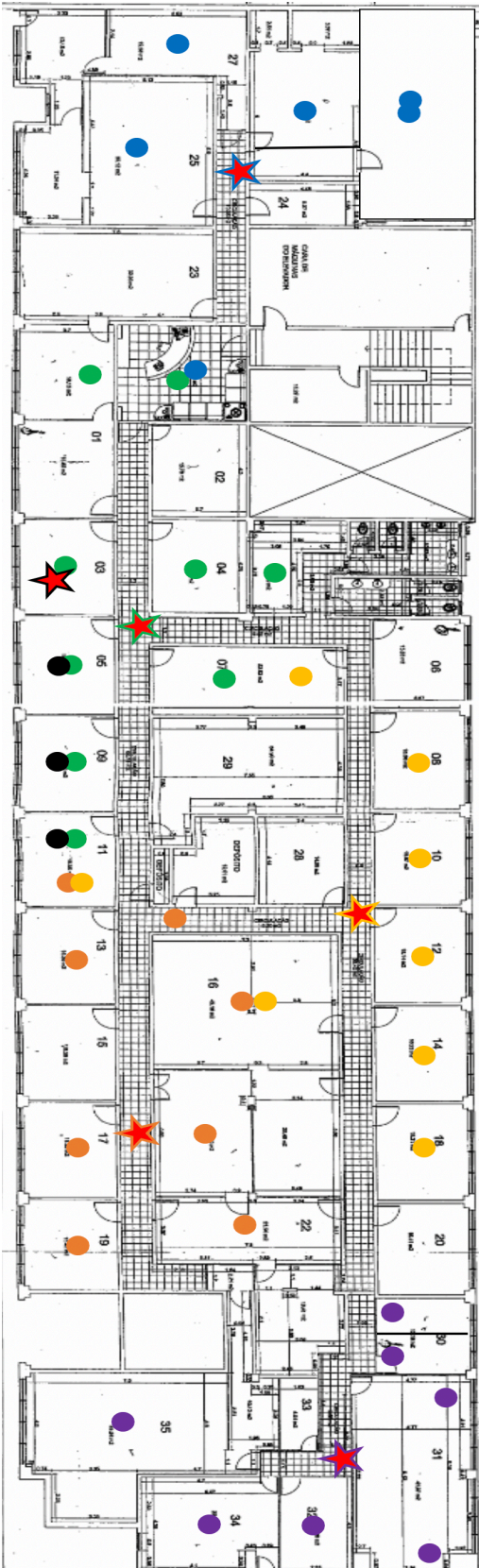
Figure 5.1: Indoor Measurements – CETUC, PUC-Rio

With TX2, two receiver points where positioned in the same location, and measurements were performed with the laboratory door open and closed. TX6 and its receiver points were positioned in order to analyze the propagation along a line, to see how much is the penetration loss through one, two and three walls.

Measurements were performed in a range of frequencies from 26.5 GHz to 40 GHz with steps of 0.5 GHz. In total, 28 frequencies were tested at the 40 receiver points. Figure 5.2 shows the path loss level for all receiver points at some frequencies. Path loss equal or lower than 120 dB are represented with green circle, values between 121 dB and 135 dB are marked with yellow circle, and path loss values higher than 135 were marked with red circle since the signal analyzer sensibility allows a maximum path loss value of 140 dB. However, above 136 dB of loss it is difficult to disguinsh signal from noise.

a)

b)

c)

Figure 5.2: Indoor Measurements at a) 28.5 GHz, b) 38 GHz, c) 40 GHz

It can be observed in Figure 5.2 that, at 28.5 GHz, 10% of the receiver points have weak signal (yellow circle) and 90% of the points have good signal (green circle). At 38 GHz, good signal points were reduced to 70%, weak signals points increased to increase to 27.5%, and it already appears one 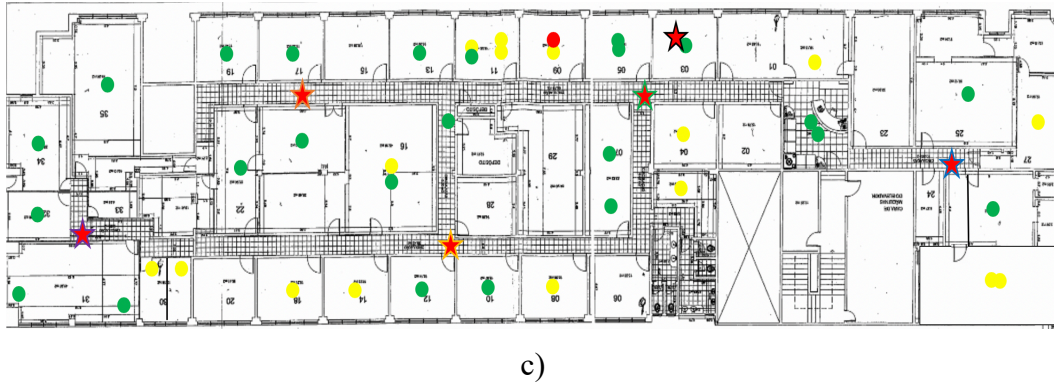receiver point (2.5%) with no-signal detected (red circle). At 40 GHz, 40% of the receiver points had weak signal, 2.5% of the points had no-signal detected and 57.5% of the points had good signal. These results, as expected, indicate that path loss tend to increase with higher frequencies even in an indoor environment, where the presence of multipaths is very high.

An interesting result come from the measurements with TX6 and its receivers. Receivers were positioned in the same line, but at different distances, crossing one, two and three walls. The link with one obstructing wall presents good signal at all frequencies. The link with two obstructing walls has good signal at 28.5 GHz, but at 38 GHz and 40 GHz no-signal was detected at reception. A metal bookcase was built-in the second wall, that explains the path loss increase in the second receiver point. Link with 3 walls has good signal at 28.5 GHz and only weak signal at 38 GHz and 40 GHz. This only can be possible due to multipath presence in the environment as the metal bookcase is still located on second wall.

Figures 5.3 to 5.5 present a comparison between the path loss models FSPL, CI and AB for the three frequencies represented in Figure 5.2. The RMSE for CI and AB models are summarized in Table 5.1. The AB model presented lower RMSE values for the three frequencies. Results are comparable with results

obtained by other researchers, considering that conical horn antennas with a gain of 20 dBi were used, with a HPBW of 16.7 degrees.

Frequency [GHz]	AB			CI	
	α	β	RMSE	n	RMSE
28.5	4.70	66.29	11.86	5.27	11.90
38.0	4.12	83.68	11.76	6.46	12.53
40.0	4.49	80.5	10.81	6.40	11.37

Table 5.1: RMSE comparison for indoor measurements.
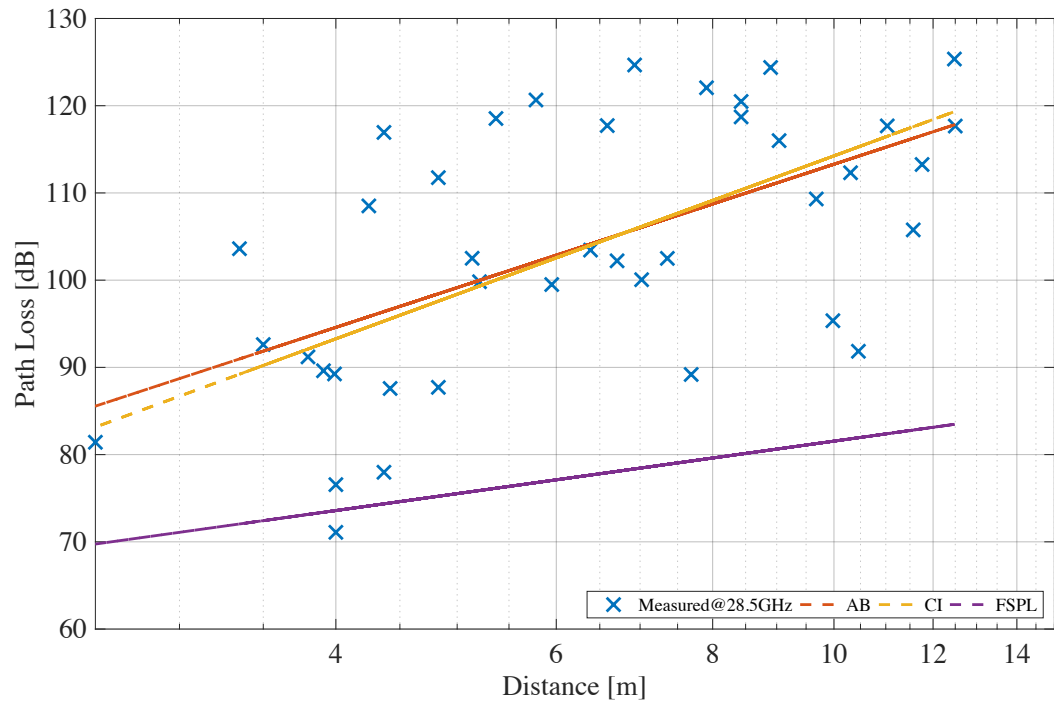
Figure 5.3: Comparison between path loss models at 28.5 GHz
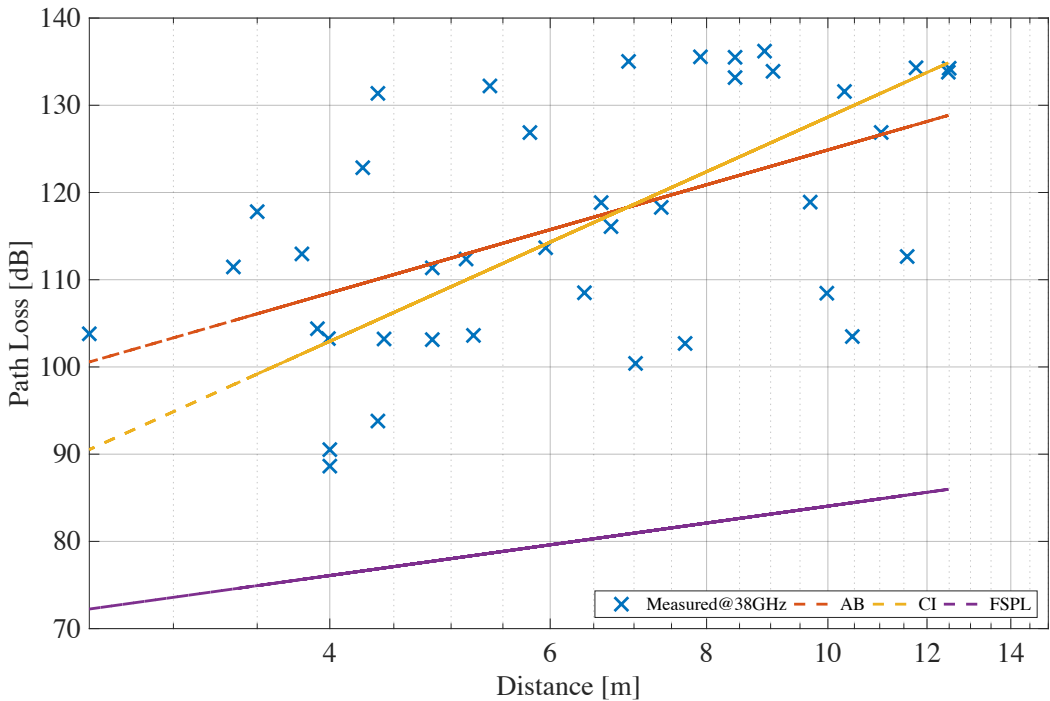
Figure 5.4: Comparison between path loss models at 38 GHz
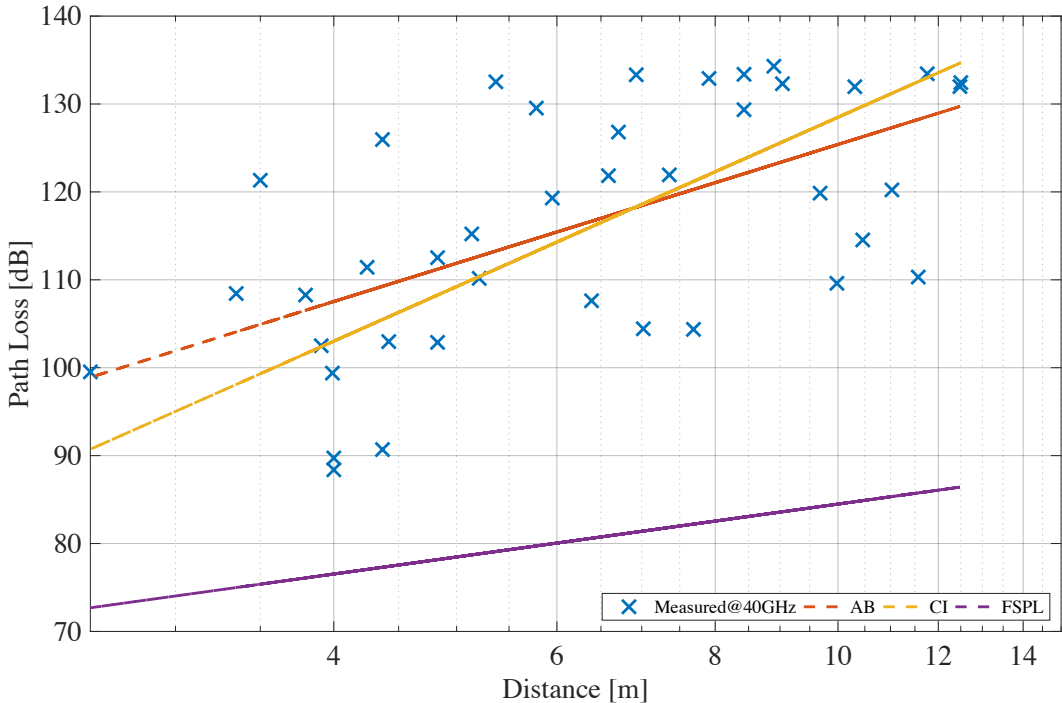
Figure 5.5: Comparison between path loss models at 40 GHz

The adjusted ABG and CIF models for this set of measurements equations (4.5) and (4.7) can be written as:

$$PL^{ABG}[dB] = 47.35 log_{10}\left(\frac{d}{1\ m}\right) + 2.4 + 48.46 log_{10}\left(\frac{f}{1\ GHz}\right) \qquad (5.1)$$

$$PL^{CIF}[dB] = PL_{FS}(f,\ d_0 = 1m)[dB] + 62.79 log_{10}(d)$$
$$+ 12.44\left(\frac{f - 32.5}{32.5}\right) log_{10}(d) \qquad (5.2)$$

The RMSE values for the adjusted ABG and CIF models are 11.33 and 11.73 respectively.

For outdoor environments, path loss dependence on frequency and distance is clear and easy to verify, as we saw in outdoor measurements section of this work. For indoor environments, because of presence of stronger multipath, the path loss dependence with distance is not so marked, as can be seen in Figures 5.6 and 5.7.
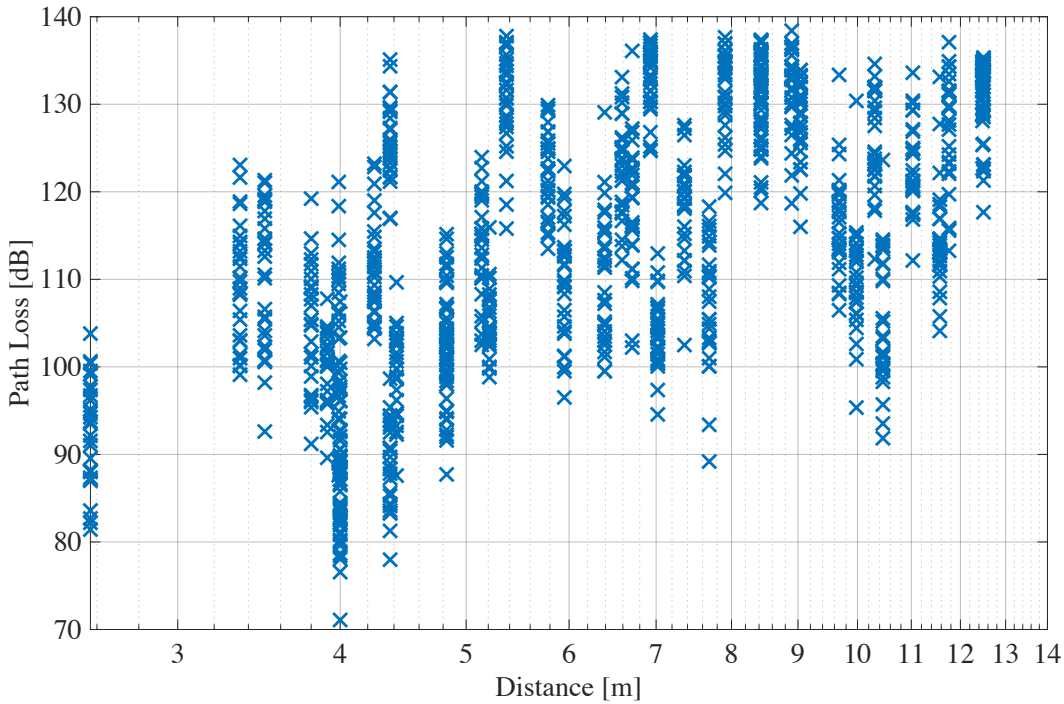
Figure 5.6: Path loss dependence on distance in indoor environments.
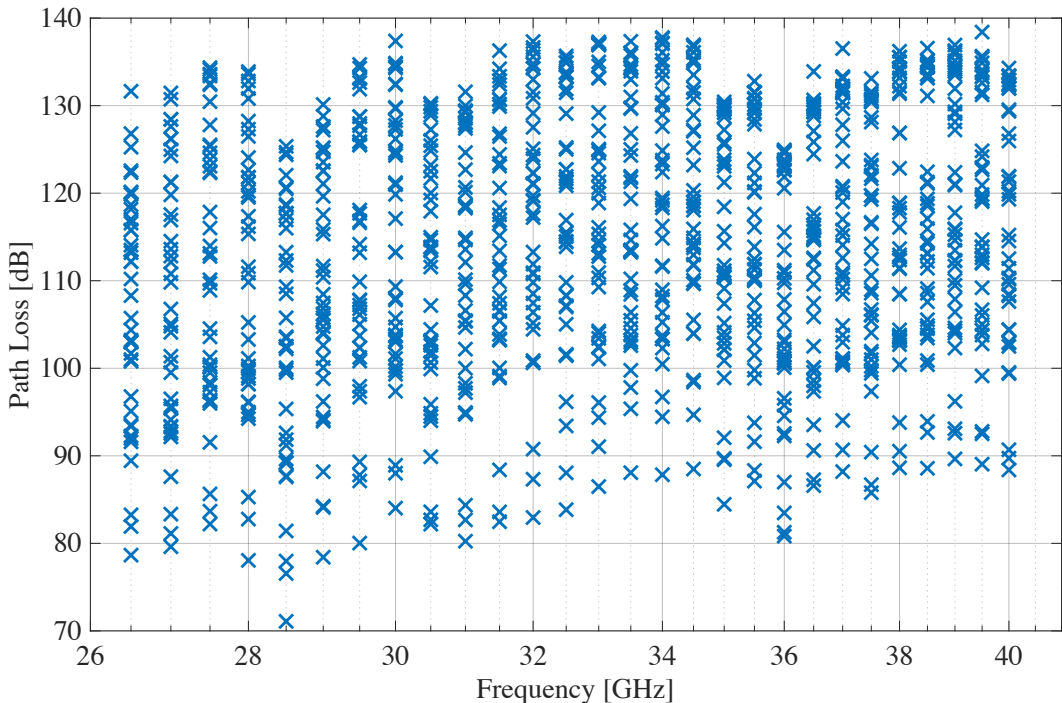
Figure 5.7: Path loss dependence on Frequency in indoor environments.

On other hand, we previously obs that walls have a high penetration loss, so as higher the walls' number, higher the path loss. The path loss dependence on walls' number, can be obd Figure 5.8.
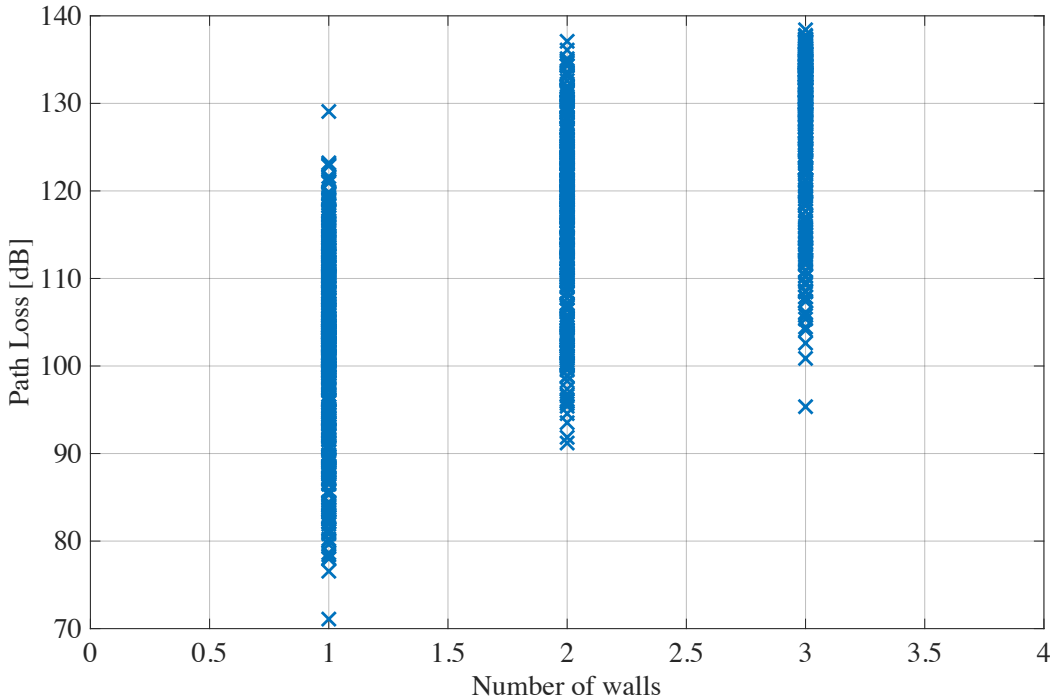
Figure 5.8: Path loss dependence on walls' number in indoor environments.

A proposed model that includes this dependence i proposed in order to reduce the RMS error. It is given by:

$$PL^{Prop}[dB] = 56.9 log_{10}(d) + 48.5 log_{10}(f) + 66.38wn - 24.31 \qquad (5.3)$$

where d is the distance between transmitter and receiver in meters, f is the frequency in GHz and wn is the walls' number between transmitter and receiver. Results for path loss comparison between predicted and measured values can be seen in Figure 5.9. Table 5.2 shows the eror results for the three models used to predict the path loss in this environment.
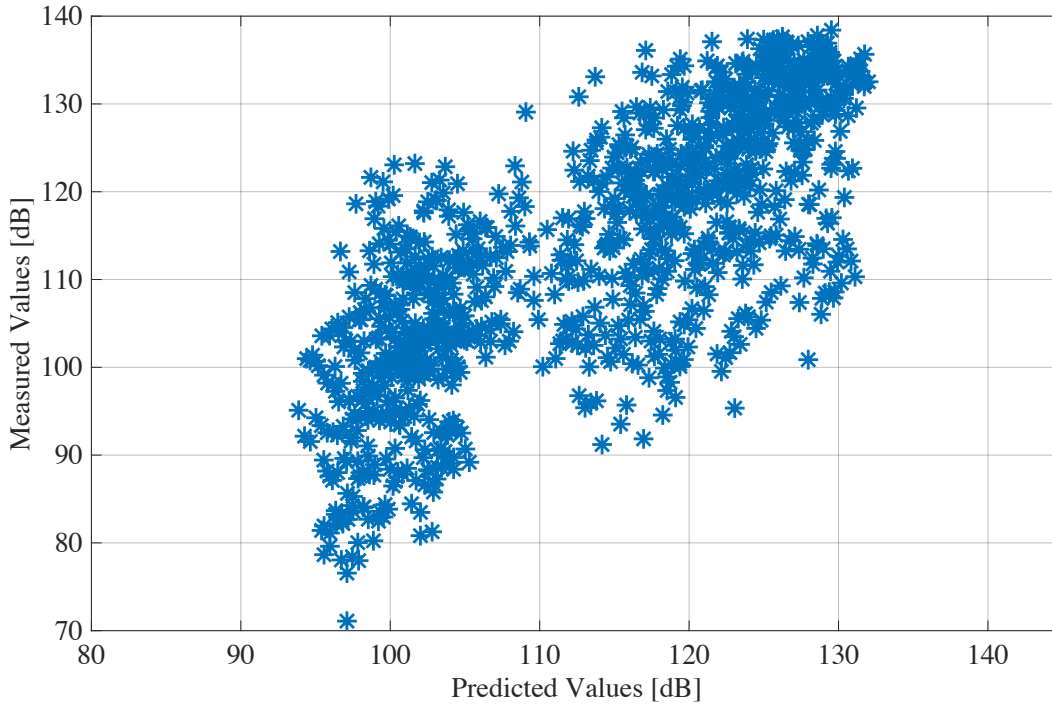
Figure 5.9: Predicted vs Measured path loss.

	α	β	γ	b	n	RMSE
ABG	4.735	2.401	4.846	-	-	11.32
CIF	-	-	-	0.198	6.27	11.72
Proposed	5.69	-24.31	4.85	66.38	-	9.17

Table 5.2: RMSE comparison for indoor measurements, single frequencies.

5.3   Measurements along a corridor

A second set of indoor measurements was performed along a corridor in one of the University buildings. The same setup as in the previous measurements was used. The signal was received at six points along the corridor separated by approximately 15 meters each, and one receiver at a point 131 meters in NLOS, as shown in Figure 5.10.

Figure 5.10: Indoor measurements along a corridor.

Figure 5.11 presents the results for the LOS-NLOS measurements at three frequencies, 28, 38 and 40 GHz. Green circles indicates path loss equal or lower than 120 dB, yellow circles indicates week signals, with $121\ dB \geq PL \leq 135\ dB$ and red circle corresponds to path loss higher than 135 dB. Transmitter is marked with a red star. It can be seen that almost all measurements at these frequencies provided good signal, even at the NLOS reception point.
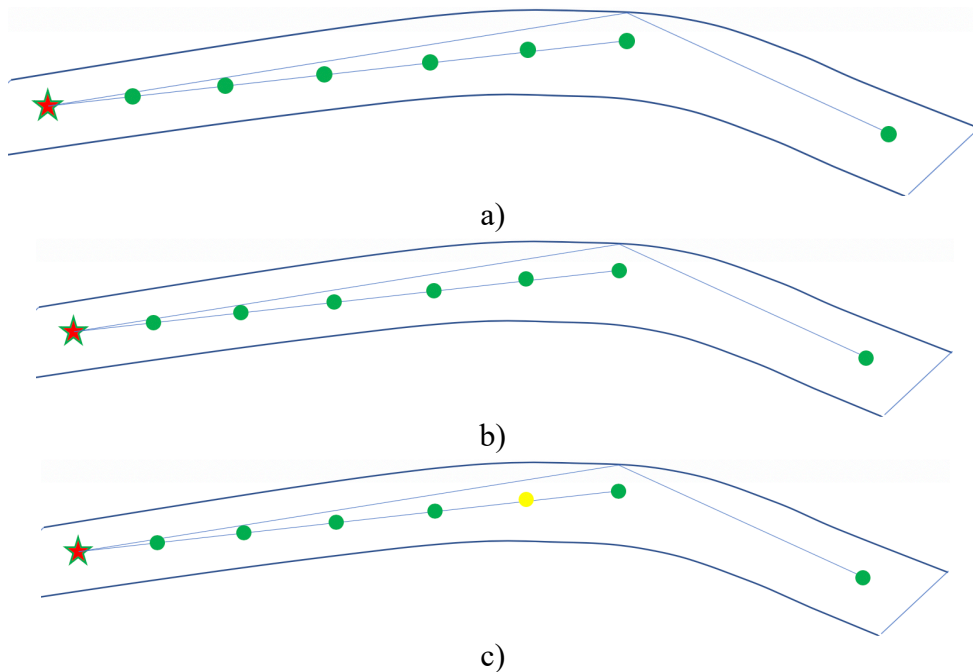
Figure 5.11: Indoor measurements along a corridor at a) 28 GHz, b) 38 GHz, c) 40 GHz

Along the corridor there are some metallic cabinets along one side of the wall. This can explain the good signal at receiver points 90 meters and 131 meters from the transmitter, and weak signal measured at 75 meters distance, as these cabinets produced strong multipath. Figure 5.12 shows the path loss dependence on frequency, from 26.5 to 40 GHz. Figure 5.13 shows the path loss dependence on distance, that clearly is stronger than dependence on frequency.
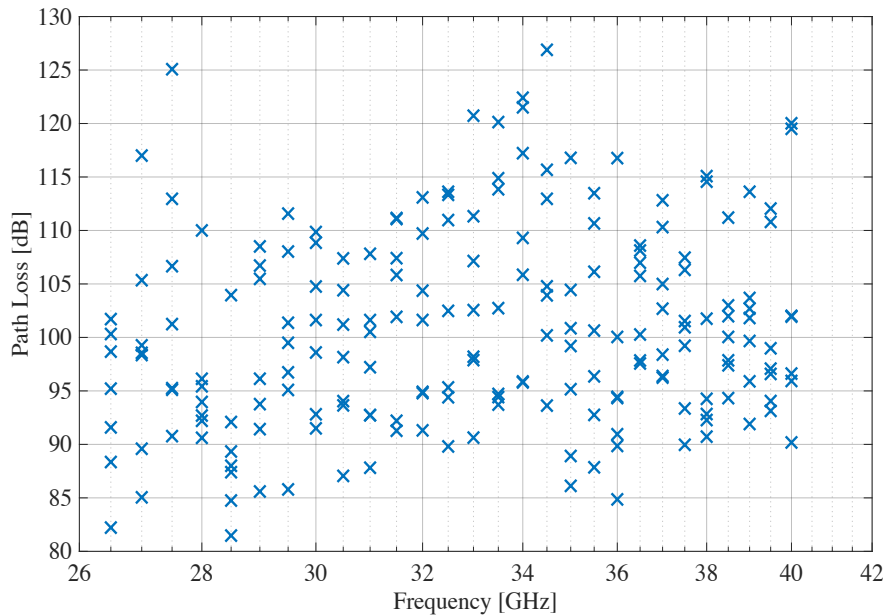
Figure 5.12: Path loss dependence on frequency along a corridor
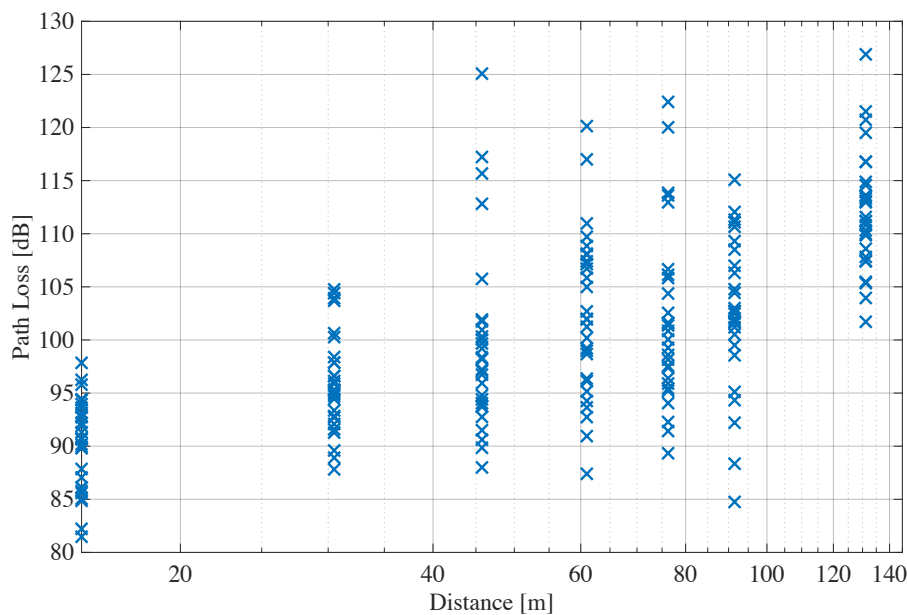
Figure 5.13: Path loss dependence on distance along a corridor

Due to few receiver points, models AB and CI cannot be compared, but models ABG and CIF can be showed for all range of frequencies. Figure 5.14 shows both path loss models.
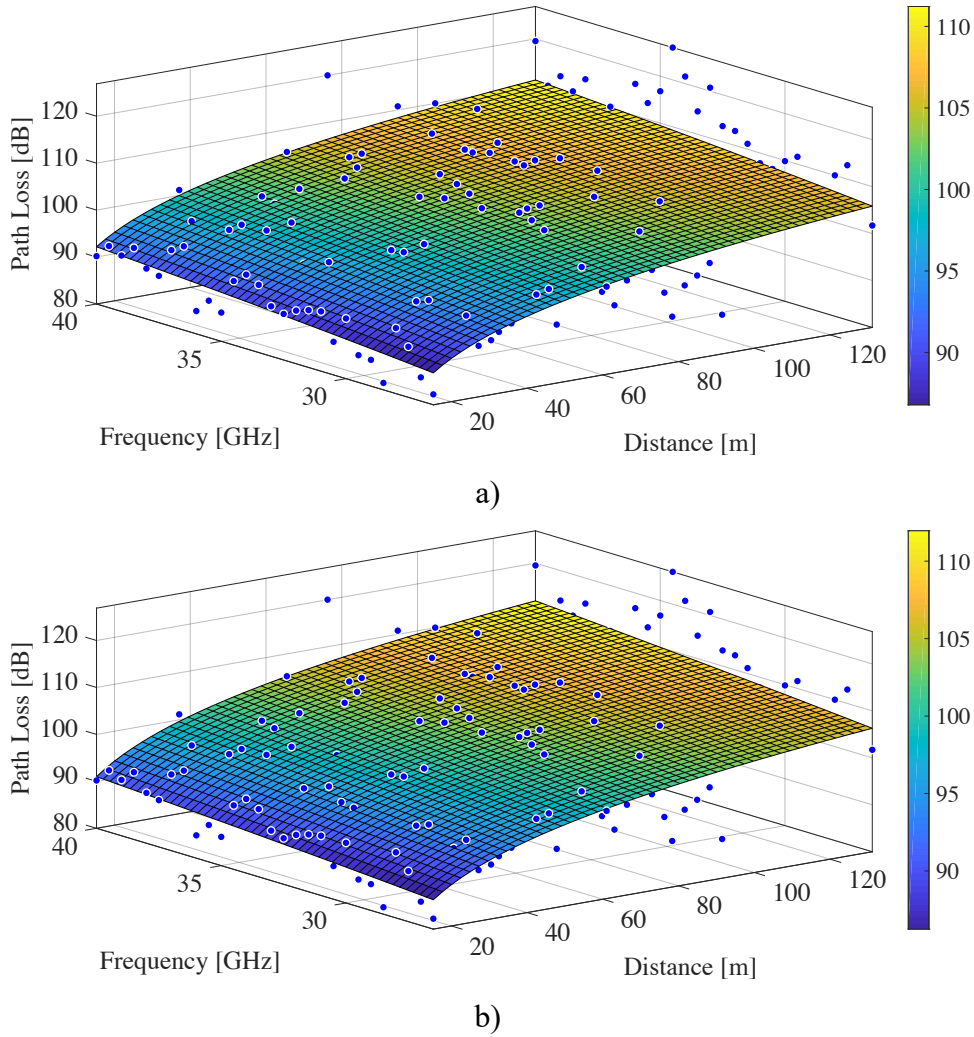
Figure 5.14: Path loss models, a) ABG c) CIF

As it can be seen in Figure 5.14, both models predict very similar results for the corridor. Coefficients and RSM error are shown in Table 5.3

	α	β	γ	b	n	**RMSE**
ABG	2.037	19.8	3.013	-	-	6.78
CIF	-	-	-	0.1084	2.189	6.79

Table 5.3: RMSE comparison for indoor measurements along a corridor.

5.4 360 degrees measurements in a corridor

A second test was performed in the corridor, at 60 meters of the transmitter, varying the Tx azimuth (0º, 15º, 345º) with the receiver azimuth varied from 0º to 360º for each Tx angle. All these measurements were done for three frequencies, 26.5 GHz, 28 GHz and 40 GHz.

Figures 5.15 to 5.17 show the path loss obtained for each angle at each frequency. As expected, path loss values at 26.5 GHz are lower than in the other two frequencies under study. Figures also show that path loss values, at all frequencies, are lower for a TX azimuth of 15 degrees as compared with 345 degrees. The presence of many reflectors in the direction of 15 degrees explains this behavior.
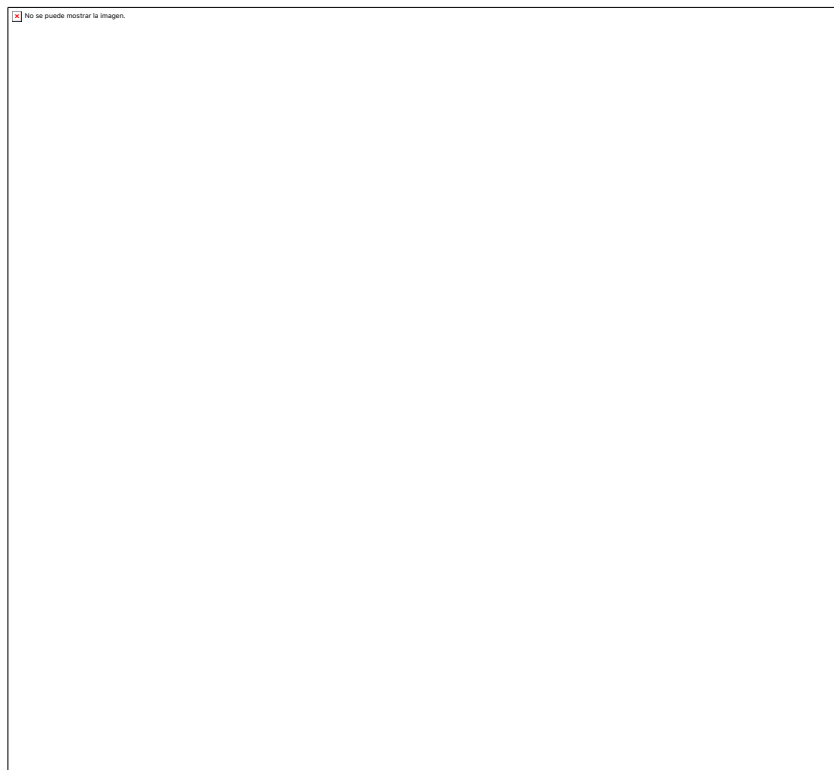
Figure 5.15: Path loss measurements in a corridor at 26.5 GHz with different TX azimuth angles and 360 degrees in RX
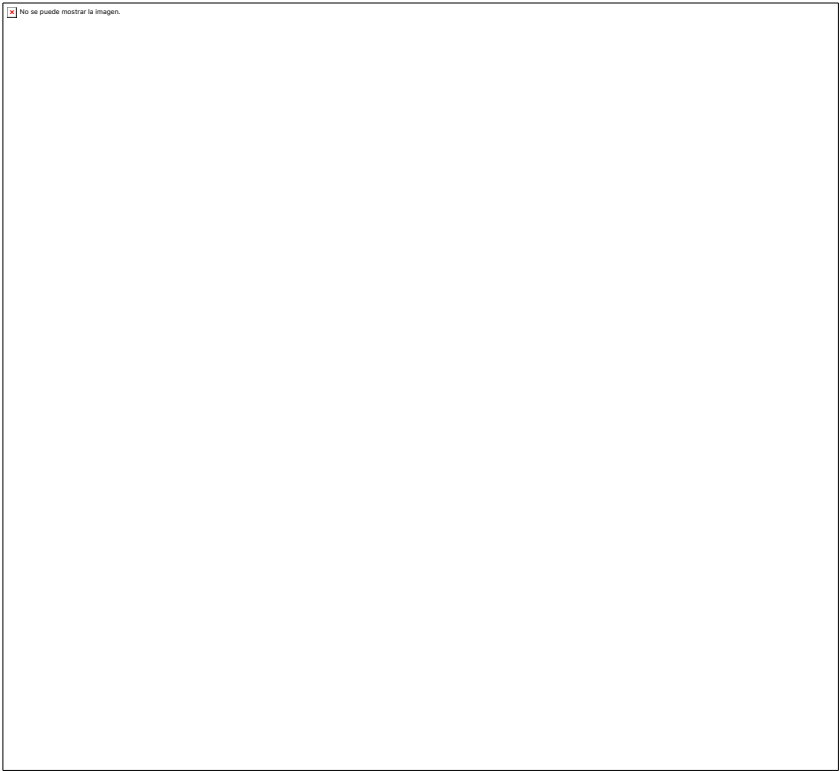
Figure 5.16: Path loss measurements in a corridor at 28 GHz with different TX azimuth
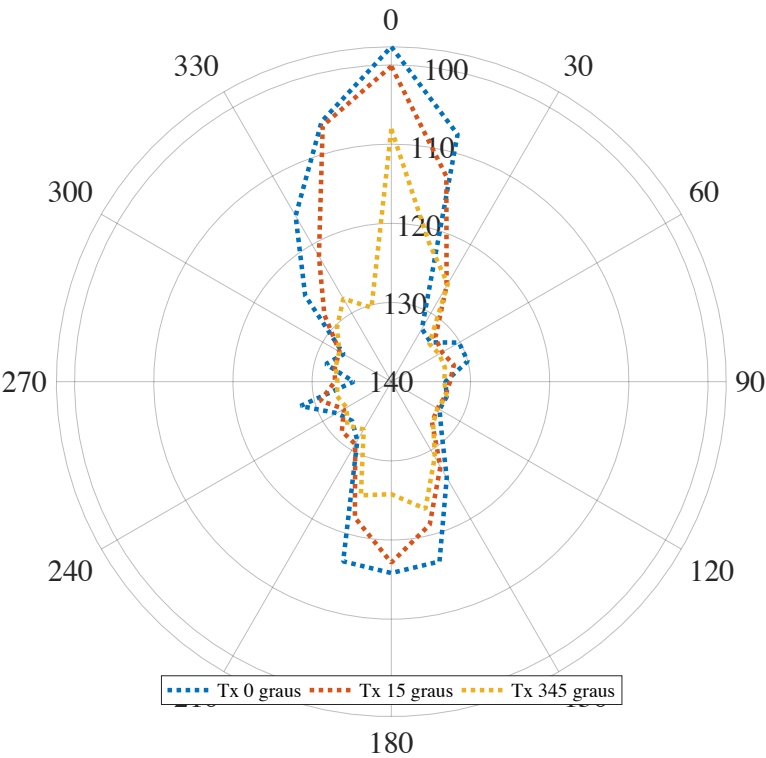
Figure 5.17: Path loss measurements in a corridor at 40 GHz with different TX azimuth angles and 360 degrees in RX

6

Conclusions

Four campaigns of transmission and reflection measurements at millimeter waves with different construction materials were performed. The first campaign was performed in a laboratory of the university, with metallic shelfs on the sides and a laminated floor. The distance between transmitter and receiver was 2 meters and the range of frequencies was from 26.5 GHz to 40 GHz, with steps of 250 MHz. Firstly, the path loss was measured in LOS situation. Then, different materials were positioned in the middle of the link and the path loss was measured again (NLOS). The difference between the path loss values was considered as the penetration loss. The materials used during measurements were thin and thick polystyrene, thin and thick pressed wood, thin and thick wood. It was verified that polystyrene presents negligible penetration loss, close to zero. A clear dependence of the material thickness was observed for both pressed wood and solid wood.

A second campaign was performed in a large meeting-room and the penetration loss of additional architectural materials was measured with the same procedure. The materials were window glass, a wooden door and a brick wall. High penetration loss was mesured for the wall, with an average of 55 dB for the whole range of frequencies. For glass, the average penetration loss was approximately 5 dB. For the wooden door, the average penetration loss was between 15 to 25 dB, depending on the thickness of the door.

As the first campaign of measurements was performed in an environment with many reflectors, the results can be biased. In order to improve the results, new campaigns were performed in three different environments to find the optimal environment for measurements. The chosen environments were a meeting room with laminated floor, a balcony semi-open environment and a terrace, which was an open area with concrete floor and walls. The distance between transmitter and

receiver was changed to one meter. The campaigns were performed for the same range of frequencies. The meeting room had a better behavior than the semi-open and open environments. Values of transmission loss for polystyrene were practically zero for all frequencies. The thin pressed wood has a penetration loss around 2 dB for the whole range of frequencies, whereas thick wood and wood had a penetration loss approximately equal to 7 dB and 4 dB, respectively.

Once the environment with better behavior for the measurements was selected, a campaign to measure the reflection coefficient of the materials was performed. Both Tx and Rx antennas were positioned in front of the material and the incidence angle was changed from 15 degrees to 45 degrees in steps of 15 degrees. Measurements were performed for the same range of frequencies. In solid wood the penetration loss is 3.57 dB at 28 GHz and 4.74 dB at 38 GHz. Reflection coefficient varies significantly with the incidence angle, from 0.137 to 0.223 at 28 GHz and from 0.223 to 0.446 at 38 GHz. Glass window presents low penetration losses at both frequencies and is the most reflective material for all incidence angles, with reflection coefficient between 0.4 to 0.7 approximately. The brick wall has the highest penetration loss and also presents high reflection coefficients, around 0.4 for all angles. The wooden door also presents high reflection coefficients, around 0.5

Results indicate that outdoor transmitted signal will hardly penetrate buildings with brick walls. Reflection coefficients indicate that indoor millimeter wave transmissions will easily be contained within rooms, reducing co-channel intercell interference.

Next, an outdoor measurement campaign was performed at the University campus for frequencies between 27 GHz and 40 GHz. One transmitter was positioned at 50 meters above ground. Receiver points inside the campus were selected and the received power level measured at each point for different frequency. Distances between transmitter and receivers goes from 54 meters to 271 meters, covering approximately 50% of the campus. As expected, coverage is much better at lower frequencies with only one point (4%) with a path loss value between

120 and 140 dB (marked as a weak signal) at 27 GHz against 26% of the points at 40 GHz. Weak signals were caused mainly by partial or total foliage blocking.

Path loss exponent was estimated for the campus environment and values vary from 2.35 to 2.65 approximately for all receiver points at 27 GHz. At 40 GHz the path loss exponent varies from 2.2 to 2.5. Then, a comparison with the AB and CI models was made and the path loss exponent obtained for majority of the frequencies is approximately 2.4. RMSE values for both models are around 4, considering the 23 receiver points, but if we exclude two receiving points, totally blocked by foliage, the RMSE values go down to 2 approximately. After that, the path loss of 21 points were estimated with ABG and CIF models and the RMSE values were 2.4 and 2.6 respectively.

With these models, we could see clearly the dependence of path loss with distance and frequency. Additionally, it is observed a dependence with the relative height between transmitter and receiver. A model considering this parameter was proposed with coefficients obtained by least square fitting to the measured data, and its equation is:

$$PL^{Prop}[dB] = 60.62 + 23.74\,log_{10}(d) + 3.56\,log_{10}(f) \\ + 4.54\,log_{10}(\Delta h/d) \tag{6.1}$$

where d is the distance between transmitter and receiver in meters, f is the frequency in GHz and Δh is the relative height between transmitter and receiver in meters. With this model, RMSE equal to 2.2 was obtained, which is lower than the RMSE values obtained with the ABG and CIF models.

It was also observed that vegetation clearly affects the obstructed links. From the 23 receiving points measured, seven links had foliage obstruction: RX1, RX2, RX4, RX10, RX16 presented partial obstruction and RX3 and RX13 had total obstruction caused by foliage. It was observed a vegetation depth dependence in the path loss. A model that includes this variable was proposed to improve our prediction model. The ABG and CIF models leads to RMSE values of 4.06 and 4.16, respectively, when considered all receiving points with and without foliage

blockage. With the proposed model, a RMSE of 2.59 was obtained. The model equation is:

$$PL^{Prop}[dB] = 53.68 + 23.23 log_{10}(d) + 8.39\, log_{10}(f)$$
$$+ 3.67\, log_{10}(\Delta h/d) + 0.47\, vd \quad\quad (6.2)$$

where d is the distance between transmitter and receiver in meters, f is the frequency in GHz, Δh is the relative height between transmitter and receiver in meters and vd is the vegetation depth. Our proposed model achieves better results than classic models. The results indicate the viability of using millimeter wave frequencies in outdoor environments with distances below 300 meters between transmitter and receiver.

The next set of measurements was performed in an indoor environment. Six transmitters positions and forty receiver points were used for this test. The environment is the Center of Studies in Telecommunications at PUC-Rio, which has laboratories for students with tables, chairs, computers, but it also has some class rooms with a larger number of chairs. The measurements were performed from 26.5 GHz to 40 GHz with steps of 500 MHz for all receiving points. At 28.5 GHz, 10% of receiver points have weak signal (path loss between 120 and 135 dB) and 90% of the points have good reception (path loss lower than 120 dB). At 38 GHz, good reception points are reduced to 70% and weak signals points increased to 27.5%. At one receiving point no-signal was detected. At 40 GHz, 40% of the reception points had weak signal reception, at 2.5% of points no-signal was detected and 57.5% of the points had good signal reception.

A second test was performed in this environment, measuring the path loss along a linear path and increasing the number of walls along the link. The link with one obstructing wall presented good signal reception at all frequencies. With two obstruction walls good signal receptions were possible at 28.5 GHz, but at 38 GHz and 40 GHz no-signal was detected due to the presence of a metallic book case against the second wall. With three obstruction walls, good signal reception was achieved at 28.5 GHz but only weak signals were measured at 38 GHz and 40 GHz.

The AB, CI, ABG and CIF model parameters were fitted to these measurements. RMSE values for all models are around 11-12 dB. Path loss exponents for this environment are around 5 to 6, which are similar to results found in the literature. It was observed a dependence with number of walls in the middle of the link, and a model including this variable was proposed:

$$PL^{Prop}[dB] = 56.9\, log_{10}(d) + 48.5\, log_{10}(f) + 66.38\, wn - 24.31 \qquad (6.3)$$

where d is the distance between transmitter and receiver in meters, f is the frequency in GHz and wn is the number of walls between transmitter and receiver. A RMSE value of 9.1 was obtained with the proposed model. Despite being high, this value is still lower than that of classic models.

The last set of measurements was performed in a corridor of a building inside the campus. A transmitter was positioned in one side of the corridor and the receiver was moved to seven different points, six of them in LOS, separated by 15 meters. The last point was located at 131 meters, in NLOS. It was observed that frequency dependence in this environment is as strong as the distance dependence. In general, it was observed good signal reception at all receiving points and at all frequencies. Few irregularities were observed at 75 meters distance, but this could be due to the presence of metallic cabinets near to this point. The ABG and CIF models were fitted and RMSE values are around 6 to 7 dB obtained for both models.

Finally, a receiver was positioned at a distance of 60 meters from the transmitter and path loss was measured in all azimuth angles from 0 (LOS) to 345 degrees with steps of 15 degrees. The azimuth in the transmitter was also changed to 15 degrees and 345 degrees (-15 degrees) and all process was repeated for each case. The measurements were performed at 26.5 GHz, 28 GHz and 40 GHz. As expected, when both antennas are with opposite directions (LOS), the lowest values of path loss were obtained. It is also observed that path loss with 15 degrees of azimuth in the transmitter has lower path loss than an azimuth of 345 degrees. This can be explained because of the presence of the metal cabinets located in the line of the 15 degrees.

All results indicate that millimeter waves are a good candidate for the next generation of mobile systems, since they propagate for short distances in indoor and outdoor environments, even with some obstructions. Outdoor systems should be limited to 200 to 300 meters and indoor systems for less than 50 meters.

References

[1]   Cisco VNI Forecast Highlights Tool, 2017

[2]   Cisco Visual Networking Index: Forecast and Trends, 2017–2022 White Paper.

[3]   Ericsson Mobility Report, November 2017

[4]   T. S. Rappaport, "The Renaissance of Wireless Communications in the Massively Broadband Era," Keynote presentation at 2012 IEEE International Conference on Communications in China (ICCC 2012), Beijing, China, Aug. 2012.

[5]   T. S. Rappaport, R. W. Heath, Jr., R. C. Daniels, and J. N. Murdock, "Millimeter Wave Wireless Communications". London, U.K.: Pearson Education, 2014.

[6]   S. Grobart, "Samsung Announces New '5G' Wireless Technology," May 2013. http://www.businessweek.com/articles/2013-05-13/samsung-announces-new- 5g-wireless-technology.

[7]   T. S. Rappaport, S. Sun, R. Mayzus, H. Zhao, Y. Azar, K. Wang, G. N. Wong, J. K. Schulz, M. Samimi, and F. Gutierrez, "Millimeter Wave Mobile Communi- cations for 5G Cellular: It Will Work!" IEEE Access Journal, vol. 1, pp. 335–349, May 2013.

[8]   Calhoun, G., Digital Cellular Radio, Artech House Inc., 1988

[9]   MacDonald, V.H., "The Cellular Concept," The Bell systems Technical Journal, Vol. 58, No. 1, pp. 15-43, January 1979.

[10]   Young, W.R., "Advanced Mobile Phone Service: Introduction, Background, and Objectives," The Bell systems Technical Journal, Vol. 58, pp. 1-14, January 1979.

[11]   Raith, K., and Uddenfeldt, J., "Capacity of Digital Cellular TDMA Systems," IEEE Transactions on Vehicular Technology, Vol. 40 No.2, pp. 323-331, May 1991

[12]   EIA/TIA Interim Standard, "Cellular System Dual Mode Mobile Station-Land Station Compatibility Specifications," IS-54, Electronic Industries Association, May 1990

[13]   Mouly, M., and Pautet, M.B., "The GSM System for Mobile Communication," ISBN: 2-9507190-0-7, 1992

[14]   TIA/ EIA Interim Standard-95, "Mobile Station-Base Station Compatibility Standard for Dual Mode Wideband Spread Spectrum Cellular System," July 1993

[15]   Personal Digital Cellular, Japanese Telecommunication System Standard, RCR STD 27.B, 1992

[16]   3GPP Release 8, http://www.3gpp.org/specifications/releases/72-release-8

[17]   3GPP Release 9, http://www.3gpp.org/specifications/releases/71-release-9

[18] 3GPP Release 10, http://www.3gpp.org/specifications/releases/70-release-10

[19] Rec. ITU-R P.676-10, "Attenuation by atmospheric gases," Sep. 2013.

[20] Rec. ITU-R P.838-3,"Specific attenuation model for rain for use in prediction methods," Sep. 2005.

[21] Rappaport, T.S. Wireless Communications Principles and Practice, 2nd ed. New Jersey: Prentice-Hall, 2002.

[22] H. Zhao, R. Mayzus, S. Sun, M. Samimi, J. K. Schulz, Y. Azar, K. Wang, G. N. Wong, F. Gutierrez Jr., and T. S. Rappaport, "28 GHz Millimeter Wave Cellular Communication Measurements for Reflection and Penetration Loss in and around Buildings in New York City," 2013 IEEE International Conference on Com- munications (ICC), Jun. 2013.

[23] T. S. Rappaport, S. Sun, R. Mayzus, H. Zhao, Y. Azar, K. Wang, G. N. Wong, J. K. Schulz, M. Samimi, and F. Gutierrez, "Millimeter Wave Mobile Communi- cations for 5G Cellular: It Will Work!" IEEE Access Journal, vol. 1, pp. 335–349, May 2013.

[24] O. Landron, M. J. Feuerstein, and T. S. Rappaport, "In Situ Microwave Reflection Coefficient Measurements for Smooth and Rough Exterior Wall Surfaces," in IEEE Vehicular Technology Conference (1993 VTC), May 18-20, 1993, Secaucus, NJ.

[25] S. Siedel, K. Shaubach, T. Tran, and T. S. Rappaport, "Research in Site- Specific Propagation Modeling for PCS System Design," 1993 IEEE Vehicular Tech- nology Conference (VTC 1993), pp. 261–264, May 1993.

[26] R. Piesiewicz, C. Jansen, S. Wietzke, D. Mittleman, M. Koch, and T. K¨urner, "Properties of building and plastic materials in the THz range," Int. J Infrared Milli. 28, 363–371 (2007).

[27] Liang Yishan ; Zhou Feng ; Sun Jinglu ; Cheng Kai ; Guo Bolun ; Wu Yong, "Analysis and measurment of wall penetration loss as a function of incident angle" 2017 International Workshop on Electromagnetics: Applications and Student Innovation Competition, May 30, 2017

[28] M. Chamchoy ; P. Jaturatussanai ; S. Promwong, "Empirically Based Path Loss and Penetration Loss Models for UWB Communication in Residential Environment", 2005 5th International Conference on Information Communications & Signal Processing, Dec 6-9, 2005

[29] G. D. Durgin, T. S. Rappaport, and H. Xu, "Partition-Based Path Loss Anal- ysis for in-Home and Residential Areas at 5.85 GHz," 1998 IEEE Global Telecom- munications Conference (GLOBECOM 1998), vol. 2, pp. 904–909, Dec. 1998.

[30] Rappaport, T.S., Xing, Y., MacCartney, G.R., Molisch, A.F., Mellios, E., Zhang,J.: 'Overview of Millimeter Wave Communications for Fifth-Generation (5G)Wireless Networks-with a focus on Propagation Models',IEEE Transactions onAntennas and Propagation, 2017,65, (12), pp. 6213–6230

[31] T. S. Rappaport et al., "Wideband millimeter-wave propagation measurements and channel models for future wireless communication system design (Invited Paper)," IEEE Transactions on Communications, vol. 63, no. 9, pp. 3029–3056, Sep. 2015.

[32] George R. MacCartney Jr., Junhong Zhang, Shuai Nie, and Theodore S. Rappaport "Path loss models for 5G millimeter wave propagation channels in urban microcells," in IEEE Global Communications Conference (GLOBECOM), Dec. 2013, pp. 3948–3953.

[33] S. Deng, M. K. Samimi, and T. S. Rappaport, "28 GHz and 73 GHz millimeter-wave indoor propagation measurements and path loss models," in 2015 IEEE International Conference on Communications (ICC), ICC Workshops, Jun. 2015.

[34] G. R. MacCartney, Jr. et al., "Indoor office wideband millimeter-wave propagation measurements and channel models at 28 GHz and 73 GHz for ultra-dense 5G wireless networks (Invited)," IEEE Access, vol. 3, pp. 2388– 2424, Dec. 2015.

[35] P. Kyösti et al., "WINNER II channel models," Eur. Commission, IST-WINNER, Tech. Rep. D1.1.2.

[36] (Sep. 2003). "Spatial channel model for multiple input multiple output (MIMO) simulations," 3rd Generat. Partnership Project, Tech. Rep. TR 25.996. [Online]. Available: http://www.3gpp.org

[37] S. Piersanti, L. A. Annoni, and D. Cassioli, "Millimeter waves chan- nel measurements and path loss models," in Proc. IEEE Int. Conf. Commun. (ICC), Jun. 2012, pp. 4552–4556.

[38] J. B. Andersen, T. S. Rappaport, and S. Yoshida, "Propagation measurements and models for wireless communications channels," IEEE Commun. Mag., vol. 33, no. 1, pp. 42–49, Jan. 1995.

[39] G. R. MacCartney, Jr., T. S. Rappaport, S. Sun, and S. Deng, "Indoor office wideband millimeter-wave propagation measurements and chan- nel models at 28 GHz and 73 GHz for ultra-dense 5G wireless networks (Invited Paper)," IEEE Access, pp. 2388–2424, Dec. 2015.